Marine Geology
August 2018, Volume 402 Pages 99-117
https://doi.org/10.1016/j.margeo.2017.09.003
https://archimer.ifremer.fr/doc/00495/60694/

Ocean-ice sheet interaction along the SE Nordic Seas margin from 35 to15 ka Bp

Becker Lukas W. M. [1, *], Sejrup Hans Petter [1], Hjelstuena Berit O. [1], Haflidason Haflidi [1], Dokken Trond M. [2, 3]

[1] Univ Bergen, Dept Earth Sci, Bergen, Norway.
[2] Uni Res, Bergen, Norway.
[3] Bjerknes Ctr Climate Res, Bergen, Norway.

* Corresponding author : Lukas W. M. Becker, email address : lwmbecker@gmail.com

Abstract :

Sediment cores from the south-eastern Nordic Seas simultaneously archive the variability of the Fennoscandian Ice Sheet (FIS), the British-Irish Ice Sheet (BIIS) and the regional oceanic conditions. This study aims to contribute to our understanding of the marine-based section of the FIS and the BIIS between 35,000 and 15,000 years BP, by using cores MD99-2283, MD99-2284 and MD99-2289, retrieved along the upper continental slope between the Faroe-Shetland Channel and the Wiring Plateau. For this, we present a revised, radiocarbon based, Bayesian modelled chronological framework and a compilation of new and published sedimentological, geochemical and micro-paleontological datasets. Our results show a possibly first Weichselian FIS/BIIS confluence at ca. 25,500 years BP in the central North Sea, which buttressed the BIIS to the East, potentially leading to a northwards BIIS deflection via the Shetlands. The Norwegian Channel Ice Stream (NCIS) most likely only reached the shelf edge after 23,300 +/- 500 years BP, possibly for the first time during the Weichselian. The NCIS onset directly preceded a pronounced influx of warm Atlantic water to the northern North Sea margin possibly implying forcing through ocean melt. We find a highly variable NCIS, with three similar to 1400 yearlong episodes of increased ice rafted debris flux interrupted by similar to 600 yearlong minima. When compared to other sides of the European Ice Sheet, these episodes appear to correlate well, suggesting a common forcing mechanism. In conclusion, our data supports recent suggestions that the last glacial stage of the BIIS was more extensive in the central North Sea and the confluence later than previously thought.

Graphical abstract

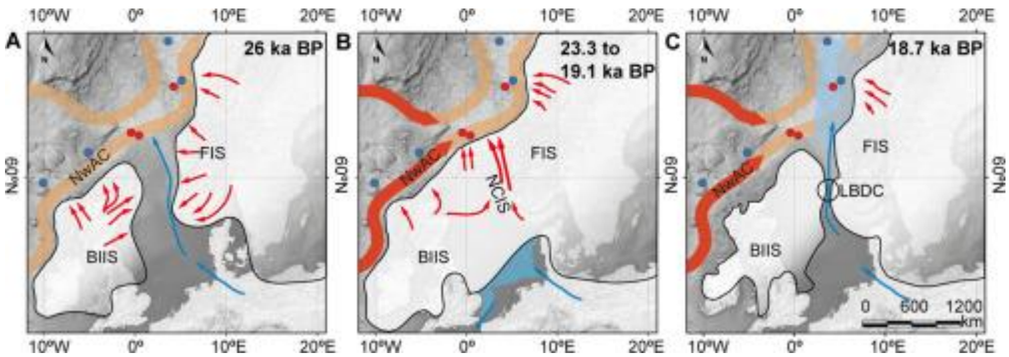

Highlights

► Possibly first, Weichselian ice confluence in the North Sea around 24.5 ± 0.3 ka BP. ► Separation of central North Sea ice dated on meltwater plume to 18.7 ± 0.2 ka BP. ► The Weichselian Norwegian Channel Ice Stream was likely restricted to 23.3–19 ka BP. ► The Ice Stream might have operated in at least three 1.5 ka long episodes. ► Episodes correlate well with S and W margins, suggesting atmospheric teleconnections.

Keywords : IRD, Multi-proxy, Norwegian Channel Ice Stream, NE Atlantic margin, Ice sheet variability, Last Glacial Maximum

1. Introduction

Large landmasses in the Northern Hemisphere have been covered repeatedly by continental ice sheets throughout the Quaternary. The world's last two continental ice sheets today, on Greenland and Antarctica, are experiencing an ongoing and, in terms of speed, possibly unprecedented loss of ice mass within the last decades, as emphasized in the last report by the Intergovernmental Panel on Climate Change (Vaughan et al., 2013). The retreat of these ice sheets, associated with potential sea level changes and the influence on the climate system, is assumed to have a large environmental impact worldwide (Vaughan et al., 2013). The increased freshwater delivery to the North Atlantic has the possible impact of reducing the strength of the Atlantic Meridional Overturning Circulation (Broecker et al., 1985; Rahmstorf et al., 2015; Liu et al., 2017), which is in turn proposed to result in large-scale restructuring of our climate system (Hall et al., 2006).

The understanding of the mechanisms controlling ice sheet decay and the associated speed of these processes, still remains fragmentary. Research on paleo-ice sheets and numerical modelling of ice sheets is today receiving increased attention in an effort to decipher the complex responses of present ice sheets to a warming climate. Within the last decade, there has been a growing focus on marine-based parts of ice sheets and their interaction with ocean circulation (Rise et al., 2005; Lekens et al., 2006; Knutz et al., 2007; Alvarez-Solas et al., 2011; Crocker et al., 2016; Wary et al., 2016). To be able to develop and test climate models, detailed knowledge about the timing and the mechanism behind the initiation, dynamics and decay of the marine-based fraction of continental ice sheets is essential (e.g. Vaughan and Arthern, 2007; Bentley et al., 2014).

The aim of this study is to contribute to our understanding of the timing of ice sheet advances and instabilities along the south-eastern Nordic Seas continental margin. This is done by compiling a series of well-dated cores from the region (Fig. 1A), covering the Middle and Late Weichselian, focusing on the time period between 35 and 15 ka before present (BP). Additionally, the observed ice sheet variability will be related to changes in ocean surface circulation in the south-eastern Nordic Seas. With this, a special focus will be set on the investigation of the timing of Norwegian Channel Ice Stream (NCIS) activity combined with new insights into the timing of British-Irish Ice Sheet (BIIS) and Fennoscandian Ice Sheet (FIS) confluence in the central North Sea.

2. Background

The Eurasian Ice Sheet, consisting of the FIS, the BIIS and the Barents-Kara Ice Sheet, encompassed a large marine-based section during maximum extension (Sejrup et al., 2005; Lee et al., 2012; Hughes et al., 2015). The location of the Eurasian Ice Sheet made it particularly vulnerable to ocean melt forcing through the inflow of warm Atlantic waters along the continental margin (Joughin et al., 2012). A high co-variability of the BIIS with changes in ocean sea surface temperature, that is, the position of the polar front, has been suggested (Scourse et al., 2009; Hall et al., 2011). Even though the maximum extension of the western oceanic border of the Eurasian Ice Sheet within the Last Glacial Maximum (LGM) is rather well documented (Dahlgren and Vorren, 2003; Sejrup et al., 2005; Clark et al., 2012; Hughes et al., 2015; Ottesen et al., 2016), the timing and structure of the build-up and deglaciation can still be refined further.

Until recently, it was widely accepted that the FIS and the BIIS were in confluence across the central North Sea between about 31-24 ka BP (Sejrup et al., 1994; Bradwell et al., 2008; Ehlers and Gibbard, 2008; Sejrup et al., 2009; Toucanne et al., 2010; Sejrup et al., 2015). Based on mapping of landforms and a compilation of data from sediment cores within the North Sea region, Sejrup et al. (2016) suggested that the two ice sheets were in confluence in the central North Sea at 23 ka BP until separating at 18.5 ka BP, but without stating the onset of confluence. Along the Mid-Norwegian margin the FIS is suggested to reach the shelf edge by 24 ka BP, marked by the deposition of glacigenic debris flows (Dahlgren et al., 2002; Dahlgren and Vorren, 2003; Hjelstuen et al., 2005).

The eastern section of the North Sea is characterized by the Norwegian Channel (Fig. 1A), a distinct ca. 850 km long morphological feature, 70-150 km in width and 280-700 m in depth (Rise et al., 2008). The morphology of the Norwegian Channel is to a large extent the product of multiple periods of ice streaming of the NCIS within the last 1.1 million years (Sejrup et al., 2003; Nygård et al., 2005; Reinardy et al., 2017). The last active period of the NCIS is reported to have taken place during the LGM and until the onset of deglaciation at around 19 ka BP (Lekens et al., 2006; Nygård et al., 2007), with estimated sediment fluxes of ca. 8,000 cubic meters per year, per meter ice front (Nygård et al., 2007). However, the onset of NCIS ice streaming during the LGM or any inter-LGM variability remains unclear and challenging to determine, as with most paleo-ice streams (Margold et al., 2015).

The timing of retreat from the maximum LGM ice stand position, that is, the shelf edge, is assumed to have differed along the north-western European margin. Studies agree on an early retreat of the BIIS along its western margin after 24 ka BP (e.g. Peck et al., 2006; Bigg et al., 2012), while the FIS along the northern North Sea margin is thought to have stayed grounded on the shelf edge until about 19 ka BP (King et al., 1998; Nygård et al., 2007; Sejrup et al., 2016). On the Mid-Norwegian margin the onset of retreat is reported to have been before 17 ka BP (Dahlgren and Vorren, 2003; Hjelstuen et al., 2005). Additionally, shell fragments in till on the same margin suggested grounded ice at the shelf edge until after 18.1 ka BP (Rokoengen and Frengstad, 1999). Following the retreat from the northern North Sea margin, recent work suggests that the NCIS had withdrawn to the innermost parts of the Norwegian Channel (Skagerrak) by 17.6 ka BP (Morén et al., 2017), which agrees with terrestrial data (Sejrup et al., 1998; Sejrup et al., 2009; Houmark-Nielsen et al., 2012; Anjar et al., 2014; Svendsen et al., 2015; Briner et al., 2016).

The along-shelf deglaciation signal is briefly halted on the Mid-Norwegian margin, where Nygård et al. (2004) describe a glacial re-advance (the Bremanger re-advance) around 16-17 ka BP onto the Måløy Plateau (Fig. 1A), which is believed to coincide with a re-advance from the Shetlands into the Fladen area (Sejrup et al., 2015).

The present-day surface current system in the studied region comprises of two branches of North Atlantic Water, the Shetland and the Faroe currents, entering the Nordic Seas across the Wyville-Thomson and the Iceland-Faroe Ridges (Hansen and Østerhus, 2000). The Shetland Current continues along the shelf edge northwards and across the Vøring Plateau as the Norwegian Atlantic Current (NwAC) (Fig. 1A). Additionally, along the coastline of Norway, the Norwegian Coastal Current transports Norwegian Coastal water northwards (Fig. 1A) (Hansen and Østerhus, 2000). Position, speed and depth of the NwAC were variable within the last glacial cycle (Rasmussen and Thomsen, 2008), with sluggish current speeds during stadials and increased flow, sorting deposits, within interstadials (Kissel et al., 1998; Dahlgren and Vorren, 2003). During the LGM, NwAC speeds along the Mid-Norwegian margin are reportedly low before the ice sheet reached the shelf edge, medium strong and able to sort sands during maximum ice advance, while strong after the onset of the last deglaciation, leading to winnowing and non-deposition (Dahlgren and Vorren, 2003).

3. Material and methods

3.1. Core locations

This study is based on a compilation of new and previously published data from the giant CALYPSO piston cores MD99-2283, MD99-2284, MD99-2289 (hereafter MD83, MD84 and MD89), raised from the south-eastern Nordic Seas margin in 1999 (Fig. 1A, Table 1). The sedimentological, geochemical, micro-paleontological and stable isotope records from these cores are compared to published data from cores MD04-2829, LINK17, MD99-2291 and MD95-2010 (Table 1) roughly taken along the approximate track of the NwAC (Fig. 1A). Together, these cores form a 1100 km long transect from Rosemary Bank, northeast of Scotland, to the northern Vøring Plateau in the eastern Norwegian Sea, enabling a spatial overview of the western margin of the Eurasian Ice Sheet, extending the work of Scourse et al. (2009) northwards.

A set of sub-bottom profiles is applied to illustrate the regional and depositional context of the studied cores (Figs. 1A and B). The profiles are a deep-towed boomer line made available by the British Geological Survey (Fig. 1C) and two 2D TOPAS high-resolution profiles (Figs. 1D and E), of which the latter is a modification of Figure 2b in Reiche et al. (2011). To convert sediment two-way-travel time into meters, we have used the velocity of 1600 m/s.

Core MD84 was retrieved from a sediment package composed of acoustically well-laminated facies, suggesting hemipelagic deposits, that appear to drape an old, deep feature (Figs. 1B and C). The eastern section of the available boomer profile (Fig. 1C) cuts through the thick package of glacigenic debris flows forming the North Sea Trough Mouth Fan. These glacigenic debris flow deposits are assumed to reflect the long history of the NCIS throughout the Quaternary (King et al., 1996; Sejrup et al., 2003;

Nygård et al., 2005). Cores MD83 and MD84 are located 75 km apart, but differ almost 800 m in water depth (Table 1). The location of core MD83 is about 40 km north-west of the shelf break, at the mouth of the Norwegian Channel (Fig. 1B) and thus downstream of the NCIS. The position of MD83 (Fig. 1D) is about 2 km west of the youngest identified glacigenic debris flows of the North Sea Trough Mouth Fan (e.g. Nygård et al., 2005).

The glacigenic debris flows appear to have protected the underlying hemipelagic sediments from the vigorous NwAC flowing along the margin (Fig. 1D), especially since the onset of the last deglaciation (Sejrup et al., 1981; Jansen et al., 1983). This can be observed by tracing the first identified reflector below the seabed from the core site of MD83 to the East (Fig. 1D), which reveals a maximum thickness of about 1.5 ms (~1 m) of hemipelagic deposits beneath the contact to the overlying glacigenic debris flow. This implies some additional time of hemipelagic sedimentation before deposition of the glacigenic debris flow, compared to the age of the core top of MD83. This observation fits well with previous work on the North Sea Fan, where the last glacigenic debris flows have been dated to have been deposited before 19.1 ka BP (King et al., 1998).

Core MD89 was raised from the south-western flank of the Vøring Plateau in a hemipelagic setting (Haflidason et al., 2003), about 100 km to the west of the last deposited glacigenic debris flows, identified on the southern part of the Vøring Plateau (Reiche et al., 2011).

3.2. Chronology

This study adds 33 new accelerator mass spectrometry (AMS) radiocarbon dates (Table 2) to the 113 previously published dates from the same cores (Table S1). In addition, the Faroe Marine Ash Zone (FMAZ) II, dated to 26.69±0.39 ka BP (Davies et al., 2008) has in this study been identified in MD83 and previously in MD84 (Dokken et al., 2013) and MD89 (Nilsen, 2014) (Table 2).

Earlier studies in the region have either constructed age models based on radiocarbon dates (e.g. Haflidason et al., 1998; Lekens et al., 2005) or have relied on tuning proxy records to Greenland ice core stratigraphies (Haflidason et al., 1995; Seierstad et al., 2014). Such tuning to Greenland Stadials and Interstadials has been based on the variability in the relative abundance of sub-polar planktonic foraminifera (e.g. Scourse et al., 2009; Hall et al., 2011; Crocker et al., 2016; Rasmussen et al., 2016), magnetic susceptibility records (e.g. Stanford et al., 2011; Dokken et al., 2013; Wary et al., 2016) or variations in relative Ca-concentration in X-Ray Fluorescence (XRF) core scanner data (Lekens et al., 2006; Brendryen et al., 2010).

In this study, all age models are based solely on radiocarbon dates. The rationale behind this is to be able to compare the proxy records from the margin to the development of the marine-based parts of the FIS and the BIIS on the continental shelf, as these records are largely based on radiocarbon dates on marine carbonates (e.g. Sejrup et al., 2016). During the age model run all dates were (re-)calibrated with Marine13 (Reimer et al., 2013), including 405-year global reservoir correction. No further local reservoir correction was applied. The changes in local reservoir effect are considered to be similar along the south-eastern Nordic Seas margin, making the presented cores comparable to each other within individual age model uncertainties.

The age models cover the time interval 40-10 ka BP (Fig. 2) and are constructed with the R-based, Bayesian age modelling script "Bacon" (v.2.2) (Blaauw and Christen, 2011). All age models were constructed with an accumulation rate distribution width of 1.5, a student-t distribution and a section thickness depending on the flexibility need in each core (Blaauw and Christen, 2011). The section thickness was set to the smallest possible value, which still allowed the age model to be run within the 2-sigma standard deviation of each calibrated radiocarbon date. Outliers were removed in core MD91 (reworking in 2 samples described in Lekens et al. (2005)), in MD89 (one sample out of context) and in MD83 (two apparently too young ages). In core MD83 the Laschamp palaeomagnetic reversal (Lekens et al., 2006) was used to constrain the age model in its oldest section. The above described FMAZII tephra was not included in any age model run and is just used to validate the tentative tuning.

The age model of core MD91 however required some additional measures, as a sudden, pronounced change in accumulation rate in the core surpasses the capabilities of Bacon. Nearly 14 m of the core is related to a rapidly deposited meltwater plume along the Mid-Norwegian margin, dated to about 18.5 ka BP (Hjelstuen et al., 2004; Lekens et al., 2005; Reiche et al., 2011; Sejrup et al., 2016; Hjelstuen et al., this issue). Thus, the previously identified "UNT6" (Reiche et al., 2011) between reflectors Ny7 (280.5 cm) and Ny6 (1720.5 cm) (Fig. 1E) was removed during age modelling in this study (Fig. 2). Through re-evaluation of core and TOPAS data, reflector Ny6 was moved to 1500 cm core depth in MD91. This section was afterwards added back into the depth scale and the sedimentation between the top and bottom point of the plume event was regarded as linear (Fig. 2). Any possible variability of the sedimentation rate within the plume can therefore not be resolved within this age model, as in fact the complete duration of the plume event itself likely lies within the age model uncertainties of about 230 years.

One of the major challenges while comparing different time series is the question of synchronicity of events, or the detection of potential leads or lags. To increase the comparability, all independent age models in this study are calculated with the same settings. Our assumption is that events are most likely synchronous if they overlap within the uncertainty of two-sigma in the age model. However, studies have attempted to solve this numerically (Werner and Tingley, 2015), or visually with "ghost plots" of any proxy within Bacon (Blaauw and Christen, 2011).

3.3. Analysis and proxies

The visual description of core MD83 was additionally supported through high resolution colour images taken with the ITRAX core scanner (COX Analytic Systems). In addition, analogue X-rays, previously taken on the split core (Lekens et al., 2006), were used to assess core stretch, voids and sediment composition.

Subsamples from all cores were wet sieved with an array of sieve sizes and in varying sampling intervals (Table 3). Most of the grain size data, however, has previously been published elsewhere. Lithic grains in the fraction >1 mm of cores MD89 and MD83 were counted manually, updating previous counts of core MD83 (Lekens et al., 2006) within the top 13 m (35-19 ka BP). Furthermore, all lithic grains in the 150-1000 μm fraction were counted in core MD83 using the automated light microscope "Morphologi G3" from Malvern Instruments (Malvern Instruments Ltd.), applying a method described in Becker et al. (Accepted Author Manuscript). In core MD84 lithic particles were manually counted in fractions >150 μm, all counts between

30 and 16.26 m core depth (35-29 ka BP) were previously published (Dokken et al., 2013). An additional 13 samples were counted in the same fraction in MD84 between 15 and 10.79 m core depth (28-25 ka BP) with the same method as for MD83. The interpretation of lithic grains >150 μm as ice rafted debris (IRD) is widely used in the literature (e.g. Bond and Lotti, 1995; Bailey et al., 2012), even though, there is an ongoing discussion on which grain size fraction should be regarded as IRD (Andrews, 2000). A study on the western Barents Sea margin associated an increased amount of IRD >500 μm with the advance and retreat of ice streams, while observing only little IRD at the maximum extension of the ice stream (Dowdeswell and Elverhøi, 2002). In this study, lithic grain counts >150 μm are interpreted as an IRD signal of a fluctuating, relatively proximal ice sheet margin.

The assemblage of planktonic foraminifera was counted in the 150-1000 μm fraction in core MD83 within the upper 13 m core depth (35-19 ka BP), with a resolution of 100-200 years. Additional samples were counted in MD89, increasing the resolution published by Berstad et al. (2003) to 200-500 years between 12.90 and 10.49 m core depth (35-27 ka BP). The high resolution (10-100 years) assemblage data from MD84 (Dokken et al., 2015b) were supplemented with 13 new counts between 11.44 and 10.79 m core depth (26-25 ka BP).

The relative concentrations of the polar species *Neogloboquadrina pachyderma* sinistral of less than 90% are widely used as an indication of influx of Atlantic water into the near surface of the Nordic Seas (Haflidason et al., 1995; Klitgaard-Kristensen et al., 2001; Austin et al., 2004; Scourse et al., 2009) indicating summer temperatures higher than 4°C (Bé and Tolderlund, 1971; Kellogg, 1980; Pflaumann et al., 2003). Previous studies suggest a change from 90% to 50% *N. pachyderma* sin. in this region to be comparable to a relative temperature variation of about 7˚C (e.g. Rasmussen and Thomsen, 2008; Dokken et al., 2013). Some data points, if based on counts of less than 200 planktonic foraminifera, were removed due to unreliability.

The oxygen stable isotope data used in this study were previously published elsewhere (Berstad, 2003; Lekens et al., 2006). The isotopes are reported in respect to the VPDB (Vienna Peedee Belemnite) standard and were measured on ca. 7 (MD83) or ca. 20 (MD84 and MD89) tests of *N. pachyderma* sin. on the Finnigan MAT251 mass spectrometer at the Geological Mass Spectrometry laboratory at the University of Bergen with an accuracy of ±0.07‰. This proxy is widely considered to partly reflect global ice volume and near-surface water freshening and/or temperature changes (e.g. Lekens et al., 2006; Rasmussen and Thomsen, 2008), where lighter values indicating fresher and/or warmer near-surface waters.

The upper 15 meters of cores MD83 and MD89, covering the studied time interval, were analysed every 500 μm on the split core with the ITRAX core scanner (COX Analytic Systems). All XRF measurements were performed with the Molybdenum tube to produce a set of relative geochemical parameters, updating earlier measurements with 40 times the previous resolution (Berstad, 2003; Lekens et al., 2006). Core MD84 was scanned every 2 cm with similar settings, but on an AVAATECH XRF core scanner. The measured counts of Calcium (Ca) were normalized with the Iron (Fe) counts. The Ca/Fe ratios were further resampled on a continuous 50 year sampling interval with the nearest point regular interpolation method of the software PAST (Hammer et al., 2001). Lekens et al. (2006) have previously demonstrated, that the Ca/Fe ratios in core MD83 closely follow the carbonate content obtained from the same core.

4. Results

The results of the performed analyses, plotted on depth scale and compared to the tentative tuning to Greenland ice core GISP2, demonstrate the large differences in accumulation rates within and between cores MD83, MD84 and MD89 (Fig. 3). In the following, the data will be presented in detail on the individual age model (Fig. 4).

4.1. Sedimentology

On average, about 80-90% of the deposits in the cores consist of silt and clay (Fig. 4). Distinct episodes with a higher content of coarser grain sizes are observed in all records. Before 26 ka BP, cores MD83 and MD84 show an influx of up to 50% very fine sorted sands for episodes of 500 to 1000 years (Figs. 4 and 5), in stark contrast to conditions after 26 ka BP, where similar influx episodes consist of coarse sand and pebbles (Figs. 4 and 6). The concentrations of grains >150 μm and >1 mm reflect this contrast, with relatively low coarse grain content before 26 ka BP and high after (Fig. 3 and 4). The coarse sediment composition after 26 ka BP is also recorded on the X-ray image of MD83 (Fig. 6), including pebbles of up to 8 cm in diameter. In MD89 the fine sand events during before 26 ka BP are not as pronounced as in the southern cores, but the relative carbonate content inferred from the Ca/Fe data (Lekens et al., 2006) shows a similar pattern as in the southern cores (Fig. 4). In MD83, the Ca/Fe data and the carbonate content correlate well with the variations in grain size composition (Fig. 5). The Ca/Fe data in MD84 display a comparable, but more complex picture (Fig. 4), with a less precise correlation of the fine sand influx and the Ca/Fe ratio. After 26 ka BP, the Ca/Fe ratio and grain size composition appear not to show any co-variability, except within an episode between 25.8 and 24.5 ka BP, a short event around 21 ka BP in MD83 and around 16 ka BP in MD89 (Fig. 4). The pronounced episodes of medium to very coarse sand influx, especially between 25.8 and 18 ka BP, are interrupted by the deposition of almost pure silt and clay grain size content. In core MD83 these episodes are most distinct (Fig. 3 and 4) and make it possible to identify three coarse influx episodes, labelled "B" (21.2-19.8 ka BP), "C" (23.5-21.6 ka BP) and "D" (25.7-24.3 ka BP). A detailed look into the IRD counts of MD84 (light yellow graph in Fig. 4) shows similar episodes and opens the possibility for a fourth, younger, episode "A" (19.3-18.3 ka BP), that is not preserved in MD83. This is in agreement with the above-mentioned observation of the erosion of hemipelagic deposits on top of MD83, which predate the adjacent glacigenic debris flow (Figs. 1D and 4).

These episodes of coarser sediment input are each about 1.5 ka in duration and are followed by 400-800 years of reduced or no coarse input (Fig. 4). Minor changes in the content of lithic grains, interpreted to be IRD, suggest higher frequency variability within each episode. The input of IRD in the more northerly located MD89 during these episodes is similar in timing, but generally less pronounced. This appearance changes between 18.5 and 15 ka BP, where increased influx of coarse sands and IRD suggests ice sheet proximity (Fig. 4). The content of IRD is largely following the variability displayed in the grain size distribution, but also gives insights into the absolute amounts of IRD flux. In all three cores the apparent episodes of IRD input between 25.8 and 18 ka BP show about four times as high a content in the oldest episode, labelled D (Fig. 4), although we note that this is less pronounced in MD89. The timing of the initiation of these episodes appears to be the same in all records, but the input differs in scale and partly in duration. The latter is believed to be a function of uncertainty within the individual age models and the above-mentioned sampling resolution.

The upper 4.5 m (26-19 ka BP) of MD83 reveal clear differences in sediment composition between the different input episodes (Fig. 6). As mentioned above, episode D appears to be different from episodes B and C. The carbonate content is slightly enhanced above average values (14%), with spikes of 16 and 20%, the magnetic susceptibility values are at their lowest (21*10^5 SI units) and the sediment is almost barren of any foraminifera (not shown). At the same time the content of lithic particles is about four times higher, even though the absolute grain size composition appears similar to episodes B and C. Additionally, it appears that episode D can be divided into two distinct periods based on the Ca/Fe ratio, sediment composition and grain counts data (Fig. 6). This episode is additionally clearly different in sediment colour, appearing much lighter than the surrounding deposits (Fig. 6). Lekens et al. (2006) published chalk counts from this core, which show a high concentration within the depth corresponding to episode D, also reflected in the relatively high carbonate content in the core. However, a re-evaluation of the coarse fraction revealed that the light-coloured grains previously interpreted to be chalk are indeed mollusc and barnacle fragments. Finally, several samples of the layer in question were analysed in an electron microscope. This confirmed the absence of any coccolithophores, making the presence of large amounts of chalk particles unlikely. The conclusion is therefore, that the increased carbonate content in episode D is likely a product of ground down mollusc and barnacle shell fragments that are present in high concentration in all size fractions (Fig. 6).

Average sedimentation rates for the studied time period are calculated to be ca. 60 cm/ka (Fig. 7), with maximum values of 350 cm/ka at around 28 ka BP in core MD89. However, this short period of very high sedimentation rates in MD89 might be an erroneous effect of age modelling through a wide spread of densely sampled radiocarbon dates at this depth (Fig. 2). Calculating the sedimentation rate between the oldest and the youngest radiocarbon date within this date cluster around 28 ka BP, yields a more reasonable sedimentation rates of 160 cm/ka.

The sedimentation rate in core MD91 exceeds 300 cm/ka at 18.7±0.23 ka BP, as 12.2 m of the core are modelled to have been deposited within only decades (Fig. 2), due to the previously described meltwater plume deposition (Reiche et al., 2011; Sejrup et al., 2016; Hjelstuen et al., this issue).

A striking feature in the calculated accumulation rates is the apparent similar change in magnitude through time within the studied cores (Fig. 7). Phases of relatively high sedimentation rates (100-150 cm/ka) in most cores are interrupted by periods of generally lower accumulation, with average rates of about 40 cm/ka, between 25.5 and 22.5 ka BP and after 18.5 ka BP.

4.2. Oceanic conditions

Throughout most of the observed time period, the polar, planktonic foraminifera *N. pachyderma* sin. generally accounts for more than 95% of the planktonic assemblage in our data (Fig. 4), suggesting full arctic conditions with close to perennial sea ice cover and near surface temperatures <4˚C (Scourse et al., 2009). This state is perturbed by several 300-900 yearlong episodes with increased presence of sub-polar species evidenced by *N. pachyderma* sin. minima of 50% in MD84, 70% in MD83 and a minimum of 80% in MD89 (Fig. 4), implying periodic influx of warm Atlantic water into the Nordic Seas (e.g. Rasmussen and Thomsen, 2008). The relative timing of these events appears to coincide between the cores, within age model uncertainties. Cores MD83 and MD89 show in general lower *N. pachyderma* sin. minima and less variability than MD84. However, the lowest values, that is, the warmest intervals in MD84, only have a duration of less than 200 years, which makes it likely that the signal is missed or blurred in MD83 and MD89, where 2 cm sample slices are taken (0.5 cm in MD84) and the sampling resolution is commonly lower than 200 years (Table 3). Arguably, MD83 and MD89 might therefore also show a higher variability when denser sampled.

The above described episodes of sorted fine sand layers in MD83 and MD84 correspond roughly with the episodes of increases in sub-polar fauna before 26 ka BP. The relative temperatures increase briefly in MD84 when the sand layers disappear (Fig. 4). This might, however, be due to a dilutive effect during deposition of the fine sands, with parts of the assemblage being possibly exposed to reworking. The rapid change in sediment composition from 50% to less than 5% fine sands at this boundary represents a large change in the depositional environment. Between 24.5 and 23.5 ka BP, two very distinctive peaks in sub-polar planktonic fauna are identified in core MD84, with *N. pachyderma* sin. minima as low as 50%. These minima coincide with similarly low values in cores MD83 (81%) and MD89 (91%). Notably, the *N. pachyderma* sin. values start to drop as soon as the coarse lithic grain content is decreasing, suggesting warm water intrusion to the coring location (Fig. 6).

5. Discussion

Based on the data presented above, the following discussion is structured into three distinct and quite different time periods in terms of the depositional environments along the studied margin. These are (Fig. 4): (1) Stadial / interstadial conditions (35-26 ka BP), (2) Full shelf edge glaciation (26-18.7 ka BP) and (3) Last deglaciation (18.7-15 ka BP).

5.1. Stadial / Interstadial conditions (35-26 ka BP)

The climate system between 35 and 26 ka BP was dominated by, periodic, large-scale temperature variations, which left a global imprint in different types of climate archives including deep sea records from the Nordic Seas (Rasmussen et al., 2016). These Greenland Interstadials (GIS) or Dansgaard-Oeschger events are characterized by rapid warming at the onsets of interstadial conditions, gradual cooling throughout the interstadial, followed by rapid cooling to stadial conditions (Dansgaard et al., 1993; Rasmussen et al., 2016). Multiple paleoclimatic proxy studies and modelling efforts have suggested a link between Dansgaard-Oeschger events and variability in Atlantic Meridional Overturning Circulation strength, sea ice extent and polar front position variations in the Nordic Seas (Elliot et al., 2002; Scourse et al., 2009; Petersen et al., 2013; Peltier and Vettoretti, 2014; Hoff et al., 2016; Rasmussen et al., 2016; Wary et al., 2016). The large-scale changes in near sea-surface temperatures along the studied transect, inferred from the relative amounts of *N. pachyderma* sin., exhibit a clear Dansgaard-Oeschger pattern before 26 ka BP (Fig. 8). This pattern is most pronounced in the southern section (Irish/Scottish margin) and not visible in the North (Mid-Norwegian margin).

The deposition of carbonate rich, sorted fine sands, coinciding with an apparent near-surface warming in cores MD83 and MD84 (Figs. 4 and 5) indicates a relatively high energy environment and the presence of Atlantic water along the margin (as described in Dahlgren and Vorren, 2003). The influx of lithic grains >150 μm through ice rafting from 35-26 ka BP is likely limited, compared to the input between 26 and 15 ka BP, where the additional presence of particles >1 mm clearly indicates ice rafting as the main contributor (Fig. 3). The apparent synchronous deposition in MD83 and MD84 coinciding with warm water influx might be due to winnowing effects of an increased overturning circulation through the Faroe-Shetland overflow during Interstadial conditions (Fig. 9A). Similar to present-day vigorous current speeds in the Faroe-Shetland Channel (Hansen and Østerhus, 2000). Sejrup et al. (1981) also described similar deposits during the Holocene, which they related to the vigorous NwAC along the upper slope in this area. An increased NwAC current speed would also agree with the stronger bio-productivity through elevated nutrient content as indicated by the increase in total planktonic foraminifera concentration during the episodes characterized by fine sand influx and higher carbonate content (Fig. 5). However, when directly comparing MD84 and MD83, with MD84 on the age model of Dokken et al. (2013), the magnetic susceptibility records appear to show the opposite behaviour (Fig. 5). The magnetic data of MD83 correlate well with the episodes of fine sand sorting and relatively warmer near-surface temperatures, linked to interstadial conditions (Lekens et al., 2006; Rasmussen and Thomsen, 2008; Scourse et al., 2009). Taking both approaches into account this would result in cores MD83 and MD84 being in anti-phase between 35-26 ka BP, despite being raised only 75 km in distance and 555 m in water depth apart. Here, the events of the two records are regarded as synchronous (Fig. 4) and the sorted fine sand influxes are seen as effects of winnowing due to an increased overturning circulation during interstadials.

Further north, along the Mid-Norwegian margin, a similar sorting effect linked with warm planktonic assemblages as seen in MD83 and MD84, is not evident in MD89 (Fig. 4). However, it has to be noted, that the sampling resolution in MD89 in this period might be too coarse (Table 3) to capture these relatively short-lived events or the distance from the overflow threshold is simply too far.

5.2. Periods with full shelf edge glaciation (26-18.7 ka BP)

After about 26 ka BP, the positive correlation between sea surface conditions, as evidenced by the *N. pachyderma* sin. content, and the fine sand flux degenerates and is replaced by a distinct change to more unsorted sediments with an increase in coarser, middle sand to pebble sized material along the transect, with no simultaneous warming of the near surface waters. This is in agreement with marine and terrestrial evidence of the onset of FIS and BIIS, switching from a mostly continental to a marine-based margin after the Ålesund/Sandnes/Denekamp interstadial around 29 ka BP (Fig. 9B) (Sejrup et al., 2000; Scourse et al., 2009; Hall et al., 2011; Mangerud et al., 2011).

The IRD influx between 26 and 18.5 ka BP does not appear to be constant, but instead varies strongly, suggesting ice sheet instabilities with alternating advances, still stands or retreats (Fig. 4), as earlier described in e.g. Hjelstuen et al. (2005) for the Mid-Norwegian margin. Such a high degree of instability for the BIIS section of the Eurasian Ice Sheet has earlier been suggested for the Irish/Scottish margin from geological evidence (Scourse et al., 2009; Haapaniemi et al., 2010; Hall et al., 2011) and also from ice sheet modelling experiments (Hubbard et al., 2009; Patton et al., 2016).

The fact that the influx episodes D-A can generally be traced along the north-western European margin suggests an overarching forcing mechanism. The first episode "D" (25.7-24.3 ka BP) is most pronounced, exhibiting the highest IRD influx from the Irish/Scottish to the Mid-Norwegian margin, even though varying in absolute amounts and exhibiting two separate peaks (Fig. 8). Earlier studies have reported a similarly pronounced event during the same time period (Dahlgren and Vorren, 2003;

Peck et al., 2006). We interpret this episode as the first widespread advance of the Eurasian Ice Sheet towards the respective shelf edges during the LGM. Simultaneously, the *N. pachyderma* sin. content suggests full arctic water temperatures during this episode, while the sediments are almost barren of foraminifera, suggesting limited productivity (Fig. 6). Episode D ends with a rapid decrease in IRD and a simultaneous rise in relative near-surface temperatures (Fig. 6 and 8), indicating a retreat of the Eurasian Ice Sheet from the shelf edge.

The reduction in IRD influx in the southern cores, following episode D, might mark the early BIIS retreat from the shelf edge as reported from other studies (e.g. Scourse et al., 2009). This is also in line with terrestrial evidence from Ireland and the United Kingdom (summarized in Hughes et al. (2015)). Scourse et al. (2009) link the rapid deterioration of the BIIS at the end of episode D to the rise in temperatures, which they correlated to GIS2. These two warming pulses at the end of episode D are clearly visible in cores MD83, MD84, LINK17 and MD04 at around 24 ka BP (Fig. 8), and is likely contributing to a substantial retreat of the calving front from the shelf edge.

The relative near-surface temperatures drop again at the onset of episode C and stay steady and low throughout the observed time period and the transect. The IRD influx north of MD83 in episode C and B is lower than during episode D, but follows similar trends as in MD83, suggesting that the FIS on the northern North Sea and Mid-Norwegian margin regained its shelf edge position within centuries, i.e., at around 23.5 ka BP. On the other hand, increased IRD influx in MD89 during episode A is not recorded, but two large influx episodes between 19 and 15 ka BP suggest late ice proximity on the Mid-Norwegian margin. South of MD83 the influx is greatly reduced after episode D (Fig. 8), supporting the above presented interpretation of the BIIS retreating from its maximum position after episode D.

The absence of further distinct warm spikes between the following episodes C-A in our data, suggests, that the apparent cyclicity of the glacial advances is at least not solely forced through increased ocean melt. Only the data from the Irish/Scottish margin suggests repeated intrusions of warm water during the period from 23 to 19 ka BP (Fig. 8), which might indicate a varying position of the polar front south of the northern North Sea margin, as suggested by Scourse et al. (2009). Especially core LINK17 exhibits relatively warm near-surface temperatures (Fig. 8), implying, that the large-scale influx of ice bergs and freshwater within this time period might have forced the path of the NwAC further westwards than suggested for pre-LGM times (Rasmussen and Thomsen, 2008).

Notably, at the same time as the data of LINK17 suggests rising near-surface temperatures, cores MD83 and MD84 show a gradual increase in the concentration of planktonic foraminifera from 24-19 ka BP (not shown), which varies in pace with the IRD influx. This could hint at improving oceanic conditions towards the end of the LGM, as proposed elsewhere (Bauch et al., 2001).

5.2.1. Norwegian Channel Ice Stream variability

The episodes of increased IRD influx in MD83, labelled B, C and D (Fig. 4) were earlier interpreted as indicators for periodic iceberg calving off the NCIS and shelf edge extension of the FIS and BIIS with an active ice stream (Lekens et al., 2006). However, the sediment composition, the high concentration of barnacle and mollusc fragments together with the other physical and geochemical parameters in MD83 (Fig. 6), and less pronounced in MD84, led us to hypothesize a provenance change between episode D and the younger episodes. If the deposits in episode D in cores MD83 and MD84 do have another provenance, this episode might offer a rare opportunity to understand the mechanisms and the timing of the NCIS onset during the LGM. Deciphering the provenance of episode D, we found three potential source regions.

Firstly, a BIIS source, which was previously suggested through the discovery of an increase in the clay mineral smectite, the presence of ordered layered clays and the above disproved chalk counts in MD83 (Lekens et al., 2006; 2009). The authors hypothesized, that the clays were an indicator for ice transport from the Moray Firth area, north-eastern Scotland. Indeed, the most proximal source for the well-preserved barnacle and mollusc shells found in episode D in MD83 (Fig. 6) is the shallow shelf area around the Shetlands, 200 km to the south-west, supporting the notion of a south-westerly provenance. Today some of the beaches on the Shetlands consist almost purely of shell sands (e.g. Whittington and Edwards, 1993). Global sea level lowering during continental ice sheet build-up at the onset of the LGM would have left an extensive area of hard substrate available for mollusc growth around the Shetlands. These mollusc banks could have subsequently been eroded through an overriding grounded ice sheet, transported to and calved off at the shelf edge, and then deposited at the coring location (Fig. 9C). This transport direction and the associated early BIIS maximum extension is in accordance with above-mentioned earlier studies interpreting this time period as the maximum extension of the BIIS (e.g. Peck et al., 2006; Bigg et al., 2012). Dating of the best-preserved and most juvenile looking mollusc fragments could help resolve this issue and confirm its hypothetical Shetland provenance, as the youngest ages would give a minimum estimate of ice expansion off the islands. Secondly, a Scandinavian, FIS origin for this mollusc-rich layer cannot be excluded, as the direct transport distance from mainland Norway is of similar magnitude. However, this would imply FIS extension to the shelf edge and across the 400 m deep Norwegian Channel at a very early stage, suggesting rapid ice sheet build-up from an ice-free coast during the Hamnsund interstadial at around 29 ka BP (Mangerud et al., 2003) to a grounded ice sheet on the shelf edge within about 1000 years, which seems unlikely. Indeed, grounded ice on the shelf edge would likely indicate an active NCIS, which is reported to transport mainly FIS sourced material (Sejrup et al., 1996). This raises the question why episodes C-A are compositionally different from D, if they all would have been delivered by the same transport mechanism. In turn, a non-Scandinavian origin for the IRD in episode D appears reasonable. Thirdly, the timing, the exceptionally high amount of IRD and, on first glance, the composition of the IRD grains, are in favour of a North American, that is, Laurentide Ice Sheet origin of the deposits. Thus, the layer might belong to North Atlantic Heinrich event 2 (H2). This would fit with observations from the western United Kingdom margin, where clear evidence of Laurentide Ice Sheet sourced material during H-events H4, H2 and H1 were found, except for H3, which is hypothesized to have a largely European contribution (Peck et al., 2007; Scourse et al., 2009; Hall et al., 2011). However, the very low magnetic susceptibility values in MD83 contradict this interpretation (Fig. 6), as H-events are commonly found to have high magnetic susceptibility values (Robinson et al., 1995). The magnetic susceptibility values are similarly low at the same time in MD84, supporting the notion, that the sediment deposited during episode D in MD84 might belong to a similar source. On the Faroe-Shetland side of the Faroe-Shetland Channel, a layer interpreted as H2 was also found to be light coloured and has a relatively low magnetic susceptibility (Ezat et al., 2014). On the other hand, the H2 deposits on the western United Kingdom margin have not been observed as such a light coloured, IRD and carbonate rich layer as in MD83 (Scourse, J., pers. comm., 2016), which underlines the interpretation, that this might be a local signal. In consequence, this episode might be a clear indication for early expansion of the BIIS to and beyond the Shetlands. Hence, the apparent difference in provenance within the episodes leads to the conclusion, that the NCIS might not have reached the outer parts of the Norwegian Channel within episode D (Fig. 9C), but rather only became more extensive after GIS2, that is, after 23.3±0.5 ka BP (Fig. 9E). This might indicate, that the NCIS was not active as an ice stream before this time during the Weichselian, which is about 4000 years later than previously suggested (Nygård, 2003). The pronounced warming on the margin in core MD83 and MD84, tentatively correlated to GIS2, precedes the proposed onset of the NCIS only briefly (Fig. 6), which could indicate forcing of the NCIS streaming through increased ocean melt.

Following on from episode D, the ice stream appears to have advanced for about 1500 years (episode C) until it came to a standstill for a couple of centuries to then advance again (episode B), followed by another pause and potentially a final advance (episode A), before retreat from the shelf edge. This interpretation is supported by the similarity of sediment composition in episodes C-A. Considering todays surface circulation patterns (Hansen and Østerhus, 2000) the north-eastwards surface transport (NwSC) along the shelf edge, allowed only a minority of the NCIS sourced icebergs to be transported south-westwards (Fig. 9E), which could explain the gradient in absolute sediment influx between MD83 and MD84.

5.2.2. FIS-BIIS confluence

Assuming that the conclusion of no NCIS activity in the northern parts of the channel before 23.3 ka BP is correct, the question is to which extent grounded ice was already reaching into the Norwegian Channel and to the shelf edge of the northern North Sea margin before that time. This conclusion effects the location and timing of FIS and BIIS confluence, which was, as described above, widely accepted to have been between about 31-24 ka BP, whereas a recent reinterpretation suggested a sustained confluence until 18.5 ka BP (Sejrup et al., 2016).

Both ice sheets are believed to gain a marine calving margin after the Ålesund/Sandnes/Denekamp interstadial. While the BIIS is interpreted to extend towards the east into the North Sea basin, the exact timing of this advance is, however, uncertain as there is a lack of datable material. Dates on the Fladen ground suggest ice proximal, but ice free conditions in the Fladen area until about 26 ka BP (Sejrup et al., 2016). On the Norwegian side, glacial ice in the northern section retreated back beyond the coastline during the Hamnsund interstadial (Mangerud et al., 2003). By 25.5 ka BP the presented data supports an eastwards extension of the BIIS from Scotland towards the North-east (Shetlands), the East (Fladen Plateau) and the South-east (Which Ground). This is interpreted to lead to confluence with the FIS, which by then extended into the Norwegian Channel, following a large-scale climatic deterioration after the Hamnsund interstadial, at the shallowest part of the Norwegian Channel, on the latitude of Stavanger, Western Norway (Fig. 9C). The timing of the confluence is therefore interpreted to be at around 25.5 ka BP, where a sharp drop in accumulation rate on the northern North Sea margin marks a sudden loss of sediment supply (Figs. 7 and 9B). This shifts earlier confluence interpretations by several thousands of years. Subsequently, the FIS and BIIS confluence potentially lead to a restructuring of the eastwards flow-direction and the BIIS was deflected north and south, delivering Shetland sourced IRD towards the region southwest of the Norwegian Channel and the location of MD83 and MD84 (25.5 to 24.5 ka BP). The observation of Shetland sourced glacial influx to the shelf edge on the northern North Sea margin in addition to the mapping of glacial landforms by Sejrup et al. (2016), suggests that the BIIS was more important for the glaciation of the central North Sea than previously anticipated. This would explain the apparent solely BIIS contribution to the northern North Sea margin around episode D (Fig. 6), as the Norwegian Channel north of the latitude of Stavanger is by then interpreted to be still mainly free of grounded ice (Fig. 8).

Evidence from freshwater drainage into the Gulf of Biscay (Toucanne et al., 2015) suggests freshwater drainage via the Fleuve Manche, when northwards transport is inhibited due to ice damming of a Eurasian Ice Sheet in confluence across the central North Sea. Finally, recent modelling efforts of the Eurasian Ice Sheet suggest a FIS and BIIS confluence around a similar latitude, with the FIS extending into the Skagerrak and the southern central North Sea about 1000 years prior to a confluence with the BIIS (Patton et al., 2016). The model comes to the same conclusion as our interpretation, with two largely independent ice sheets that merely "meet" in the eastern parts of the central North Sea and buttress each other during that time period. We interpret from the presented data that the NCIS reached the shelf edge about 1000-1500 years after initial confluence (Fig. 9D) at the start of episode C, roughly around 23.3 ka BP (Figs. 9E and 8).

The BIIS and the FIS are thus believed to be in confluence between 25.5±0.3 and 18.7±0.2 ka BP and therefore much later than the previously suggested 30-25 ka BP (Bradwell et al., 2008; Sejrup et al., 2009). The earlier described Tampen advance at around 21 ka BP (Sejrup et al., 2015) would by this interpretation not be a separate advance of the FIS, but instead the late, first advance of the FIS across the Norwegian Channel during the LGM. Advances into the Måløy area on the Mid-Norwegian margin are inferred to around 16 ka BP, the earlier described Bremanger event (Nygård et al., 2004).

5.3. Last deglaciation (18.7-15 ka BP)

The onset of deglaciation and as such the retreat of the grounded ice from the shelf edge is interpreted to have initiated at around 19 ka BP through a speed up in ice streaming through the NCIS (Nygård et al., 2007). This resulted in a draw down and thinning of the ice sheet in the central North Sea area (Sejrup et al., 2016) leading finally to the separation of the FIS and the BIIS. Sejrup et al. (2016) proposed that the separation is marked by the collapse of an ice dam in the central North Sea, which was holding back the ice-dammed lake in the southern North Sea. This lake is then interpreted to subsequently have drained northwards through the Ling Bank Drainage Channel (Fig. 9F). In favour of this, north of the North Sea Trough Mouth Fan an acoustically transparent unit, interpreted as a meltwater plume (in cores MD89, MD91 and MD2010), was mapped by Hjelstuen et al. (2004) and later described by several studies (Hjelstuen et al., 2005; Lekens et al., 2005; Reiche et al., 2011). This suspension plume is interpreted to originate from a point source in the direction of the Norwegian Channel (Lekens et al., 2005) and was, as discussed above, likely deposited within only centuries. This, including a detailed view in the fluvial deposits within the Norwegian Channel and the delta build up on the Ling Bank is further discussed in Hjelstuen et al. (this issue).

The timing of the deposition of the meltwater plume on the Mid-Norwegian margin is dated to 18.7±0.2 ka BP in the three presented and independently age modelled cores MD89, MD91 and MD2010 (green line in Fig. 8). Within the oxygen isotope data, a 1‰ step in the cores on the Mid-Norwegian margin precedes a long 2‰ light oxygen isotope event in all cores by about 500 years (Fig. 8). The light isotope event in all cores between 18 and 15 ka BP likely shows the global, post LGM deglaciation signal.

We interpret the 1‰ step, most pronounced in MD91, as a trace of the freshwater perturbation of the glacially dammed lake collapse, released through the Ling Bank Drainage Channel (Sejrup et al., 2016; Hjelstuen et al., this issue). Hjelstuen et al. (this issue) estimate the duration of lake drainage to be only 5-15 months.

During deglaciation, the high IRD influx in MD89 and, to a lesser extent to MD91, after 19 ka BP appears to be restricted to the Mid-Norwegian margin (Fig. 8). This is in agreement with observations of a delayed deglaciation signal north of the North Sea Trough Mouth Fan and the mentioned Bremanger re-advance at around 16-17 ka BP (Nygård et al., 2004).

5.4. Regional implications

Comparing the above discussed IRD influx episodes D-A along the northern North Sea shelf edge with studies from the southern and the western (Irish) margin of the Eurasian Ice Sheet (Fig. 1A), there appears to be a good correlation between the individual events (Fig. 10). In fact, while anticipating a constant local reservoir correction of 1000 years for the presented age models, which is in agreement with the chronological offset of the FMAZII tephra layers (Table 2), episodes D-A have an almost perfect fit with riverine runoff events in the Gulf of Biscay (Ménot et al., 2006; Toucanne et al., 2015) and IRD flux spikes off western Ireland (Peck et al., 2008) (Fig. 1A). These time series are displayed on tuned, absolute chronologies. The riverine runoff events within the Gulf of Biscay (Fig. 1A) are interpreted as implications of Eurasian Ice Sheet fluctuations within the Baltics and the southern North Sea, e.g. the southern, continental margin of the Eurasian Ice Sheet (Toucanne et al., 2015). On the western margin, Peck et al. (2008) record the advance and retreat signal off western Ireland (Fig. 1A), agreeing with terrestrial and Irish/Scottish shelf studies on the retreat pattern (e.g. Peters et al., 2015). Offsets between the dataset in this study and the other data cannot be evaluated due to the large reservoir effect uncertainties. Under the assumption of age model comparability, it appears that all margins of the southern Eurasian Ice Sheet act simultaneous to one common forcing. Interestingly, as already indicated by Peck et al. (2008), a similar pattern (b-a in Fig. 10) is found throughout the southern North Atlantic (Bond and Lotti, 1995). Therefore, the forcing mechanism and the teleconnections might potentially not only be confined to the Eurasian Ice Sheet, but rather to the whole North Atlantic region, connecting influx from the Laurentide Ice Sheet and the Eurasian Ice Sheet. Additionally, the fact that not only marine margins appear to show the same signal, but also continental margins (Toucanne et al., 2015) strongly indicates atmospheric teleconnections as at least one important driver of these simultaneous changes.

6. Conclusions

Our compilation of new and previously published, well-dated cores, enables us to makes inferences about ice-sheet advances and instabilities along the south-eastern Nordic Seas continental margin and link this with the variability in ocean circulation between 35 and 15 ka BP. The established chronology, based on 146 AMS radiocarbon dates, is regarded as coherent within the presented transect of cores, but as no delta R correction has been applied, it should be emphasized that the absolute age of parts of the records may be significantly younger. The identification of the tephra FMAZII, dated to 26.7±0.4 cal. ka BP, suggests that the delta R at this time might have been close to +1000 years, confirming previously suggested reservoir ages in the region (Davies et al., 2008).

The following conclusions can be drawn from the analysed sedimentological, geochemical and micro-paleontological proxies in this study:

- Between 35 and 26 ka BP, the stadial/interstadial deposition pattern along the northern North Sea margin is characterized by 500-1000 year long periods dominated by strong current speeds with winnowing effects and periods which are influenced by glacimarine deposition.
- The possibly first Weichselian confluence of the FIS and the BIIS at 25.5±0.3 ka BP is marked by a sharp drop in accumulation rates along the margin, suggesting cut-off from southern sediment sources. The confluence is interpreted to have lasted until the last inter-ice sheet connection collapsed in the central North Sea, releasing a rapidly deposited meltwater plume onto the Mid-Norwegian margin, which we dated in three cores to 18.7±0.2 ka BP.

- Following the confluence, we propose a possibly first time BIIS expansion northeast of the Shetlands within the Weichselian, between 25.5 and 24.5 ka BP. This is evidenced by a distinct change in sediment provenance on the northern North Sea margin.
- The change in provenance on the northern North Sea margin led us to suggest a late extension of grounded ice in the northern section of the Norwegian Channel, potentially restricting the only Weichselian NCIS activity to between 23.3±0.5 ka BP and 19.0 ka BP. We noted that the onset of the NCIS directly precedes a large-scale intrusion of warm near-surface waters into the study region, which may indicate forcing through ocean melt.
- Strong variations in the IRD flux on the northern North Sea margin indicate a highly variable NCIS, consisting of at least three streaming/advancing episodes, interrupted by 500-600 yearlong halts/retreats.
- The presented four episodes of high IRD flux on the northern Eurasian Ice Sheet margin compared to similar data off the western and eastern Eurasian Ice Sheet margin may indicate a common glacial forcing mechanism and potential atmospheric teleconnections.

7. Acknowledgements

The research leading to these results has received funding from the GLANAM (GLAciated North Atlantic Margins) Initial Training Network, a People Program (Marie Curie Actions) of the European Union's Seventh Framework Program FP7/2007-2013 under REA grant agreement n° 317217. This work was additionally supported by the gender program ("likestillingsprogrammet") at the University of Bergen to B. O.

Hjelstuen. All sediment analyses were done at the national infrastructure EARTHLAB (NRC 226171) at the University of Bergen. The authors acknowledge I. Berstad and T. Nilsen for the data of core MD99-2289. V. Hope, T. Richter, J. Kuvås, A. J.-G. Becker and H. Kinkel are thanked for their extensive laboratory work, B. Reinardy and B. Robson are thanked for language editing. Olex AS and the British Geological Survey ©NERC are thanked for their kind permission to use their bathymetric and shallow seismic data. Finally, the authors thank two anonymous reviewers for their helpful input.

References

Alvarez-Solas, J., Montoya, M., Ritz, C., Ramstein, G., Charbit, S., Dumas, C., Nisancioglu, K., Dokken, T. and Ganopolski, A., 2011. Heinrich event 1: an example of dynamical ice-sheet reaction to oceanic changes. Climate of the Past, 7(4): 1297-1306.

Andrews, J., 2000. Icebergs and iceberg rafted detritus (IRD) in the North Atlantic: facts and assumptions. Oceanography, 13(3): 100-108.

Anjar, J., Larsen, N.K., Håkansson, L., Möller, P., Linge, H., Fabel, D. and Xu, S., 2014. A 10Be-based reconstruction of the last deglaciation in southern Sweden. Boreas, 43: 132-148.

Austin, W.E.N., Wilson, L.J. and Hunt, J.B., 2004. The age and chronostratigraphical significance of North Atlantic Ash Zone II. Journal of Quaternary Science, 19(2): 137-146.

Bailey, I., Foster, G.L., Wilson, P.A., Jovane, L., Storey, C.D., Trueman, C.N. and Becker, J., 2012. Flux and provenance of ice-rafted debris in the earliest Pleistocene sub-polar North Atlantic Ocean comparable to the last glacial maximum. Earth Planet. Sci. Lett., 341: 222-233.

Bauch, H.A., Erlenkeuser, H., Spielhagen, R., Struck, U., Matthiessen, J., Thiede, J. and Heinemeier, J., 2001. A multiproxy reconstruction of the evolution of deep and surface waters in the subarctic Nordic seas over the last 30,000 yr. Quaternary Science Reviews, 20: 659-678.

Bé, A.W.H. and Tolderlund, D.S., 1971. Distribution and ecology of living planktonic foraminifera in surface waters of the Atlantic and Indian Oceans. In: B.M. Funnel and W.R. Riedel (Editors), The Micropaleontology of Oceans, pp. 105-149.

Becker, L.W.M., Hjelstuen, B.O., Støren, E.W.N. and Sejrup, H.P., Accepted Author Manuscript. Automated counting of sand sized particles in marine records. Sedimentology.

Bentley, M.J., Ó Cofaigh, C., Anderson, J.B., Conway, H., Davies, B., Graham, A.G.C., Hillenbrand, C.-D., Hodgson, D.A., Jamieson, S.S.R., Larter, R.D., Mackintosh, A., Smith, J.A., Verleyen, E., Ackert, R.P., Bart, P.J., Berg, S., Brunstein, D., Canals, M., Colhoun, E.A., Crosta, X., Dickens, W.A., Domack, E., Dowdeswell, J.A., Dunbar, R., Ehrmann, W., Evans, J., Favier, V., Fink, D., Fogwill, C.J., Glasser, N.F., Gohl, K., Golledge, N.R., Goodwin, I., Gore, D.B., Greenwood, S.L., Hall, B.L., Hall, K., Hedding, D.W., Hein, A.S., Hocking, E.P., Jakobsson, M., Johnson, J.S., Jomelli, V., Jones, R.S., Klages, J.P., Kristoffersen, Y., Kuhn, G., Leventer, A., Licht, K., Lilly, K., Lindow, J., Livingstone, S.J., Massé, G., McGlone, M.S., McKay, R.M., Melles, M., Miura, H., Mulvaney, R., Nel, W., Nitsche, F.O., O'Brien, P.E., Post, A.L., Roberts, S.J., Saunders, K.M., Selkirk, P.M., Simms, A.R., Spiegel, C., Stolldorf, T.D., Sugden, D.E., van der Putten, N., van Ommen, T., Verfaillie, D., Vyverman, W., Wagner, B., White, D.A., Witus, A.E. and Zwartz, D., 2014. A community-based geological reconstruction of Antarctic Ice Sheet deglaciation since the Last Glacial Maximum. Quaternary Science Reviews, 100: 1-9.

Berstad, I.M., 2003. Quaternary climate variability in the eastern Nordic Sea region inferred from speleotherm and deep-sea cores. PhD Thesis, University of Bergen, Bergen, Norway, 140 pp.

Berstad, I.M., Sejrup, H.P., Klitgaard-Kristensen, D. and Haflidason, H., 2003. Variability in temperature and geometry of the Norwegian Current over the past 600 yr; stable isotope and grain size evidence from the Norwegian margin. Journal of Quaternary Science, 18(7): 591-602.

Bigg, G.R., Clark, C.D., Greenwood, S.L., Haflidason, H., Hughes, A.L.C., Levine, R.C., Nygard, A. and Sejrup, H.P., 2012. Sensitivity of the North Atlantic circulation to break-up of the marine sectors of the NW European ice sheets during the last Glacial: A synthesis of modeling and palaeoceanography. Global and Planetary Change, 98-99: 153-165.

Blaauw, M. and Christen, J.A., 2011. Flexible Paleoclimate Age-Depth Models Using an Autoregressive Gamma Process. Bayesian Analysis, 6: 457-474.

Bond, G.C. and Lotti, R., 1995. Iceberg Discharges into the North Atlantic on Millennial Time Scales During the Last Glaciation. Science, 267(5200): 1005-10.

Bradwell, T., Stoker, M.S., Golledge, N.R., Wilson, C.K., Merritt, J.W., Long, D., Everest, J.D., Hestvik, O.B., Stevenson, A.G., Hubbard, A.L., Finlayson, A.G. and Mathers, H.E., 2008. The northern sector of the last British Ice Sheet: Maximum extent and demise. Earth-Science Reviews, 88(3-4): 207-226.

Brendryen, J., Haflidason, H. and Sejrup, H.P., 2010. Norwegian Sea tephrostratigraphy of marine isotope stages 4 and 5: Prospects and problems for tephrochronology in the North Atlantic region. Quaternary Science Reviews, 29(7-8): 847-864.

Briner, J.P., Goehring, B.M., Mangerud, J. and Svendsen, J.I., 2016. The deep accumulation of 10Be at Utsira, southwestern Norway: Implications for cosmogenic nuclide exposure dating in peripheral ice sheet landscapes. Geophysical Research Letters, 43.

Broecker, W., Peteet, D.M. and Rind, D., 1985. Does the ocean-atmosphere system have more than one stable mode of operation? Nature, 315: 21-26.

Clark, C.D., Hughes, A.L.C., Greenwood, S.L., Jordan, C. and Sejrup, H.P., 2012. Pattern and timing of retreat of the last British-Irish Ice Sheet. Quaternary Science Reviews, 44: 112-146.

Crocker, A.J., Chalk, T.B., Bailey, I., Spencer, M.R., Gutjahr, M., Foster, G.L. and Wilson, P.A., 2016. Geochemical response of the mid-depth Northeast Atlantic Ocean to freshwater input during Heinrich events 1 to 4. Quaternary Science Reviews, 151: 236-254.

Dahlgren, K.I.T., Vorren, T.O. and Laberg, J.S., 2002. Late Quaternary glacial development of the mid-Norwegian margin—65 to 68°N. Marine and Petroleum Geology, 19(9): 1089-1113.

Dahlgren, K.I.T. and Vorren, T.O., 2003. Sedimentary environment and glacial history during the last 40 ka of the Vøring continental margin, mid-Norway. Marine Geology, 193: 93-127.

Dansgaard, W., Johnsen, S.J., Clausen, H.B., Dahljensen, D., Gundestrup, N.S., Hammer, C.U., Hvidberg, C.S., Steffensen, J.P., Sveinbjornsdottir, A.E., Jouzel, J. and Bond, G., 1993. Evidence for General Instability of Past Climate from a 250-Kyr Ice-Core Record. Nature, 364(6434): 218-220.

Davies, S.M., Wastegard, S., Rasmussen, T.L., Svensson, A., Johnsen, S.J., Steffensen, J.P. and Andersen, K.K., 2008. Identification of the Fugloyarbanki tephra in the NGRIP ice core: a key tie-point for marine and ice-core sequences during the last glacial period. Journal of Quaternary Science, 23(5): 409-414.

Dokken, T., Andersson, C. and Risebrobakken, B., 2015a. Relative abundance of planktic foraminifera and calculated SSTs and SST anomaly (11.1-25.5 ka BP) in sediment core MD95-2010. PANGAEA.DOI: 10.1594/PANGAEA.841922

Dokken, T., Andersson, C. and Risebrobakken, B., 2015b. Relative abundance of planktic foraminifera and calculated SSTs and SST anomaly (0-25.5 ka BP) in sediment core MD99-2284.DOI: 10.1594/PANGAEA.846924

Dokken, T.M. and Jansen, E., 1999. Rapid changes in the mechanism of ocean convection during the last glacial period. Nature, 401(6752): 458-461.

Dokken, T.M., Nisancioglu, K.H., Li, C., Battisti, D.S. and Kissel, C., 2013. Dansgaard-Oeschger cycles: Interactions between ocean and sea ice intrinsic to the Nordic seas. Paleoceanography, 28(3): 491-502.

Dowdeswell, J.A. and Elverhøi, A., 2002. The timing of initiation of fast-flowing ice streams during a glacial cycle inferred from glacimarine sedimentation. Marine Geology, 188: 3-14.

Ehlers, J. and Gibbard, P., 2008. Extent and chronology of Quaternary glaciation. Episodes, 31(2): 211-218.

Elliot, M., Labeyrie, L. and Duplessy, J.C., 2002. Changes in North Atlantic deep-water formation associated with the Dansgaard–Oeschger temperature oscillations (60–10 ka). Quaternary Science Reviews, 21: 1153-1165.

Ezat, M.M., Rasmussen, T.L. and Groeneveld, J., 2014. Persistent intermediate water warming during cold stadials in the southeastern Nordic seas during the past 65 k.y. Geology, 42(8): 663-666.

Haapaniemi, A.I., Scourse, J.D., Peck, V.L., Kennedy, H., Kennedy, P., Hemming, S.R., Furze, M.F.A., Pienkowski, A.J., Austin, W.E.N., Walden, J., Wadsworth, E. and Hall, I.R., 2010. Source, timing, frequency and flux of ice-rafted detritus to the Northeast Atlantic margin, 30-12 ka: testing the Heinrich precursor hypothesis. Boreas, 39(3): 576-591.

Haflidason, H., Sejrup, H.P., Kristensen, D.K. and Johnsen, S., 1995. Coupled Response of the Late-Glacial Climatic Shifts of Northwest Europe Reflected in Greenland Ice Cores - Evidence from the Northern North-Sea. Geology, 23(12): 1059-1062.

Haflidason, H., King, E.L. and Sejrup, H.P., 1998. Late Weichselian and Holocene sediment fluxes of the northern North Sea Margin. Marine Geology, 152(1-3): 189-215.

Haflidason, H., Sejrup, H.P., Berstad, I.M., Nygård, A., Richter, T., Bryn, P., Lien, R. and Berg, K., 2003. A Weak Layer Feature on the Northern Storegga Slide Escarpment, European Margin Sediment Dynamics.

Hall, I.R., Moran, S.B., Zahn, R., Knutz, P.C., Shen, C.C. and Edwards, R.L., 2006. Accelerated drawdown of meridional overturning in the late-glacial Atlantic triggered by transient pre-H event freshwater perturbation. Geophysical Research Letters, 33(16).

Hall, I.R., Colmenero-Hidalgo, E., Zahn, R., Peck, V.L. and Hemming, S.R., 2011. Centennial- to millennial-scale ice-ocean interactions in the subpolar northeast Atlantic 18-41 kyr ago. Paleoceanography, 26(2): 1-18.

Hammer, Ø., Harper, D.A.T. and Ryan, P.D., 2001. PAST: Paleontological Statistics Software Package for Education and Data Analysis. Palaeontologia Electronica, 4(1).

Hansen, B. and Østerhus, S., 2000. North Atlantic–Nordic Seas exchanges. Progess in Oceanography, 45: 109-208.

Hjelstuen, B., Sejrup, H.P., Haflidason, H., Nygård, A., Berstad, I.M. and Knorr, G., 2004. Late Quaternary seismic stratigraphy and geological development of the south Vøring margin, Norwegian Sea. Quaternary Science Reviews, 23: 1847-1865.

Hjelstuen, B.O., Petter Sejrup, H., Haflidason, H., Nygård, A., Ceramicola, S. and Bryn, P., 2005. Late Cenozoic glacial history and evolution of the Storegga Slide area and adjacent slide flank regions, Norwegian continental margin. Marine and Petroleum Geology, 22(1-2): 57-69.

Hjelstuen, B.O., Sejrup, H.P., Valvik, E. and Becker, L.W.M., this issue. Evidence of a ice-dammed lake outburst in the North Sea during the last deglaciation. Marine Geology.

Hoff, U., Rasmussen, T.L., Stein, R., Ezat, M.M. and Fahl, K., 2016. Sea ice and millennial-scale climate variability in the Nordic seas 90 kyr ago to present. Nature Communications, 7: 12247.

Houmark-Nielsen, M., Linge, H., Fabel, D., Schnabel, C., Xu, S., Wilcken, K.M. and Binnie, S., 2012. Cosmogenic surface exposure dating the last deglaciation in Denmark: Discrepancies with independent age constraints suggest delayed periglacial landform stabilisation. Quaternary Geochronology, 13: 1-17.

Hubbard, A., Bradwell, T., Golledge, N.R., Hall, A.M., Patton, H., Sugden, D.E., Cooper, R. and Stoker, M.S., 2009. Dynamic cycles, ice streams and their impact on the extent, chronology and deglaciation of the British–Irish ice sheet. Quaternary Science Reviews, 28: 758-776.

Hughes, A.L.C., Gyllencreutz, R., Lohne, Ø.S., Mangerud, J. and Svendsen, J.I., 2015. The last Eurasian ice sheets – a chronological database and time-slice reconstruction, DATED-1. Boreas, 10(1111).

Jansen, E., Sejrup, H.P., Fjaeran, T., Hald, M., Holtedahl, H. and Skarbo, O., 1983. Late Weichselian Paleoceanography of the Southeastern Norwegian Sea. Norsk Geologisk Tidsskrift, 63(2-3): 117-146.

Joughin, I., Alley, R.B. and Holland, D.M., 2012. Ice-sheet response to oceanic forcing. Science, 338(6111): 1172-6.

Kellogg, T.B., 1980. Paleoclimatology and Paleo-Oceanography of the Norwegian and Greenland Seas - Glacial-Interglacial Contrasts. Boreas, 9(2): 115-137.

King, E.L., Sejrup, H.P., Haflidason, H., Elverhøi, A. and Aarseth, I., 1996. Quaternary seismic stratigraphy of the North Sea Fan: glacially fed gravity flow aprons, hemipelagic sediments, and large submarine slides. Marine Geology, 130: 293-315.

King, E.L., Haflidason, H., Sejrup, H.P. and Løvlie, R., 1998. Glacigenic debris flows on the North Sea Trough Mouth Fan during ice stream maxima. Marine Geology, 152(1-3): 217-246.

Kissel, C., Laj, C., Mazaud, A. and Dokken, T., 1998. Magnetic anisotropy and environmental changes in two sedimentary cores from the Norwegian sea and the North Atlantic. Earth and Planetary Science Letters, 164(3-4): 617-626.

Klitgaard-Kristensen, D., Sejrup, H.P. and Haflidason, H., 2001. The last 18 kyr fluctuations in Norwegian Sea surface conditions and implications for the magnitude of climatic change: Evidence from the North Sea. Paleoceanography, 16(5): 455-467.

Knutz, P.C., Zahn, R. and Hall, I.R., 2007. Centennial-scale variability of the British Ice Sheet: Implications for climate forcing and Atlantic meridional overturning circulation during the last deglaciation. Paleoceanography, 22(1): 1-14.

Lee, J.R., Busschers, F.S. and Sejrup, H.P., 2012. Pre-Weichselian Quaternary glaciations of the British Isles, The Netherlands, Norway and adjacent marine areas south of 68˚N: implications for long-term ice sheet development in northern Europe. Quaternary Science Reviews, 44: 213-228.

Lekens, W.A.H., Sejrup, H.P., Haflidason, H., Petersen, G.O., Hjelstuen, B. and Knorr, G., 2005. Laminated sediments preceding Heinrich event 1 in the Northern North Sea and Southern Norwegian Sea: Origin, processes and regional linkage. Marine Geology, 216(1-2): 27-50.

Lekens, W.A.H., Sejrup, H.P., Haflidason, H., Knies, J. and Richter, T., 2006. Meltwater and ice rafting in the southern Norwegian Sea between 20 and 40 calendar kyr BP: Implications for Fennoscandian Heinrich events. Paleoceanography, 21(3): PA3013.

Lekens, W.A.H., Haflidason, H., Sejrup, H.P., Nygard, A., Richter, T., Vogt, C. and Frederichs, T., 2009. Sedimentation history of the northern North Sea Margin during the last 150 ka. Quaternary Science Reviews, 28(5-6): 469-483.

Liu, W., Xie, S.P., Liu, Z. and Zhu, J., 2017. Overlooked possibility of a collapsed Atlantic Meridional Overturning Circulation in warming climate. Sci Adv, 3(1).

Malvern Instruments Ltd., 2017. Morphologi G3 - Advanced particle characterization made easy

Mangerud, J., Løvlie, R., Gulliksen, S., Hufthammer, A.K., Larsen, E. and Valen, V., 2003. Paleomagnetic correlations between Scandinavian Ice-Sheet fluctuations and Greenland Dansgaard–Oeschger events, 45,000–25,000 yr B.P. Quaternary Research, 59: 213-222.

Mangerud, J., Gyllencreutz, R., Lohne, Ø. and Svendsen, J.I., 2011. Glacial History of Norway. 15: 279-298.

Margold, M., Stokes, C.R. and Clark, C.D., 2015. Ice streams in the Laurentide Ice Sheet: Identification, characteristics and comparison to modern ice sheets. Earth-Science Reviews, 143: 117-146.

Ménot, G., Bard, E., Rostek, F., Weijers, J.W.H., Hopmans, E.C., Schouten, S. and Sinninghe Damsté, J.S., 2006. Early Reactivation of European Rivers During the Last Deglaciation. Science, 313.

Morén, B.M., Sejrup, H.P., Hjelstuen, B.O., Borge, M.V. and Schäuble, C., 2017. The last deglaciation of the Norwegian Channel; geomorphology, stratigraphy and radiocarbon dating. Boreas.

Nilsen, T.E., 2014. Kronologi, askestratigrafi og utbredelse av store askeutbrudd fra de siste 40 ka i kjerne MD99-2289 fra Norskehavet. MSc Thesis, University of Bergen, Bergen, 114 pp.

Nygård, A., 2003. Pleistocene sedimentary processes and glacial history of the Southern Norwegian continental margin. PhD Thesis, University of Bergen, Bergen.

Nygård, A., Sejrup, H.P., Haflidason, H., Cecchi, M. and Ottesen, D., 2004. Deglaciation history of the southwestern Fennoscandian Ice Sheet between 15 and 13 14C ka BP. Boreas, 33: 1-17.

Nygård, A., Sejrup, H.P., Haflidason, H. and Bryn, P., 2005. The glacial North Sea Fan, southern Norwegian Margin: architecture and evolution from the upper continental slope to the deep-sea basin. Marine and Petroleum Geology, 22: 71-84.

Nygård, A., Sejrup, H.P., Haflidason, H., Lekens, W.A.H., Clark, C.D. and Bigg, G.R., 2007. Extreme sediment and ice discharge from marine-based ice streams: New evidence from the North Sea. Geology, 35(5): 395-398.

Ottesen, D., Stokes, C.R., Bøe, R., Rise, L., Longva, O., Thorsnes, T., Olesen, O., Bugge, T., Lepland, A. and Hestvik, O.B., 2016. Landform assemblages and sedimentary processes along the Norwegian Channel Ice Stream. Sedimentary Geology, 338: 115-137.

Patton, H., Hubbard, A., Andreassen, K., Winsborrow, M. and Stroeven, A.P., 2016. The build-up, configuration, and dynamical sensitivity of the Eurasian ice-sheet complex to Late Weichselian climatic and oceanic forcing. Quaternary Science Reviews, 153: 97-121.

Peck, V.L., Hall, I.R., Zahn, R., Elderfield, H., Grousset, F., Hemming, S.R. and Scourse, J.D., 2006. High resolution evidence for linkages between NW European ice sheet instability and Atlantic Meridional Overturning Circulation. Earth and Planetary Science Letters, 243(3-4): 476-488.

Peck, V.L., Hall, I.R., Zahn, R., Grousset, F., Hemming, S.R. and Scourse, J.D., 2007. The relationship of Heinrich events and their European precursors over the past 60 ka BP: a multi-proxy ice-rafted debris provenance study in the North East Atlantic. Quaternary Science Reviews, 26(7-8): 862-875.

Peck, V.L., Hall, I.R., Zahn, R. and Elderfield, H., 2008. Millennial-scale surface and subsurface paleothermometry from the northeast Atlantic, 55-8 ka BP. Paleoceanography, 23(3): n/a-n/a.

Peltier, W.R. and Vettoretti, G., 2014. Dansgaard-Oeschger oscillations predicted in a comprehensive model of glacial climate: A “kicked” salt oscillator in the Atlantic. Geophysical Research Letters, 41: 7306-7313.

Peters, J.L., Benetti, S., Dunlop, P. and Ó Cofaigh, C., 2015. Maximum extent and dynamic behaviour of the last British–Irish Ice Sheet west of Ireland. Quaternary Science Reviews, 128: 48-68.

Petersen, S.V., Schrag, D.P. and Clark, P.U., 2013. A new mechanism for Dansgaard-Oeschger cycles. Paleoceanography, 28(1).

Pflaumann, U., Sarnthein, M., Chapman, M., d'Abreu, L., Funnell, B., Huels, M., Kiefer, T., Maslin, M., Schulz, H., Swallow, J., van Kreveld, S., Vautravers, M., Vogelsang, E. and Weinelt, M., 2003. Glacial North Atlantic: Sea-surface conditions reconstructed by GLAMAP 2000. Paleoceanography, 18(3): 1065.

Rahmstorf, S., Box, J.E., Feulner, G., Mann, M.E., Robinson, A., Rutherford, S. and Schaffernicht, E.J., 2015. Exceptional twentieth-century slowdown in Atlantic Ocean overturning circulation. Nature Climate Change, 5(5): 475-480.

Rasmussen, T.L. and Thomsen, E., 2008. Warm Atlantic surface water inflow to the Nordic seas 34-10 calibrated ka BP. Paleoceanography, 23(1).

Rasmussen, T.L., Thomsen, E. and Moros, M., 2016. North Atlantic warming during Dansgaard-Oeschger events synchronous with Antarctic warming and out-of-phase with Greenland climate. Nature Scientific Reports, 6: 20535.

Reiche, S., Hjelstuen, B.O. and Haflidason, H., 2011. High-resolution seismic stratigraphy, sedimentary processes and the origin of seabed cracks and pockmarks at Nyegga, mid-Norwegian margin. Marine Geology, 284(1-4): 28-39.

Reimer, P.J., Bard, E., Bayliss, A., Beck, J.W., Blackwell, P.G., Ramsey, C.B., Buck, C.E., Cheng, H., Edwards, R.L., Friedrich, M., Grootes, P.M., Guilderson, T.P., Haflidason, H., Hajdas, I., Hatte, C., Heaton, T.J., Hoffmann, D.L., Hogg, A.G., Hughen, K.A., Kaiser, K.F., Kromer, B., Manning, S.W., Niu, M., Reimer, R.W., Richards, D.A., Scott, E.M., Southon, J.R., Staff, R.A., Turney, C.S.M. and van der Plicht, J., 2013. Intcal13 and Marine13 Radiocarbon Age Calibration Curves 0-50,000 Years Cal Bp. Radiocarbon, 55(4): 1869-1887.

Reinardy, B.T.I., Hjelstuen, B.O., Sejrup, H.P., Augedal, H. and Jørstad, A., 2017. Late Pliocene-Pleistocene environments and glacial history of the northern North Sea. Quaternary Science Reviews, 158: 107-126.

Rise, L., Ottesen, D., Berg, K. and Lundin, E., 2005. Large-scale development of the mid-Norwegian margin during the last 3 million years. Marine and Petroleum Geology, 22(1-2): 33-44.

Rise, L., Bøe, R., Ottesen, D., Longva, O. and Olsen, H.A., 2008. Postglacial depositional environments and sedimentation rates in the Norwegian Channel off southern Norway. Marine Geology, 251(1-2): 124-138.

Risebrobakken, B., Dokken, T., Smedsrud, L.H., Andersson, C., Jansen, E., Moros, M. and Ivanova, E.V., 2011. Early Holocene temperature variability in the Nordic Seas: The role of oceanic heat advection versus changes in orbital forcing. Paleoceanography, 26.

Risebrobakken, B., Dokken, T., Smedsrud, L.H., Andersson, C., Jansen, E., Moros, M. and Ivanova, E.V., 2014. (Table 1) Age determination of Barents Sea sediment cores, Supplement to: Risebrobakken, B et al. (2011): Early Holocene temperature variability in the Nordic Seas: The role of oceanic heat advection versus changes in orbital forcing. Paleoceanography, 26(4), PA4206, https://doi.org/10.1029/2011PA002117. PANGAEA.10.1594/PANGAEA.829724

Robinson, S.G., Maslin, M.A. and Mccave, I.N., 1995. Magnetic-Susceptibility Variations in Upper Pleistocene Deep-Sea Sediments of the Ne Atlantic - Implications for Ice Rafting and Paleocirculation at the Last Glacial Maximum. Paleoceanography, 10(2): 221-250.

Rokoengen, K. and Frengstad, B., 1999. Radiocarbon and seismic evidence of ice-sheet extent and the last deglaciation on the mid-Norwegian continental shelf. Norsk Geologisk Tidsskrift, 79(2): 129-132.

Scourse, J.D., Haapaniemi, A.I., Colmenero-Hidalgo, E., Peck, V.L., Hall, I.R., Austin, W.E.N., Knutz, P.C. and Zahn, R., 2009. Growth, dynamics and deglaciation of the last British-Irish ice sheet: the deep-sea ice-rafted detritus record. Quatern. Sci. Rev., 28(27-28): 3066-3084.

Seierstad, I.K., Abbott, P.M., Bigler, M., Blunier, T., Bourne, A.J., Brook, E., Buchardt, S.L., Buizert, C., Clausen, H.B., Cook, E., Dahl-Jensen, D., Davies, S.M., Guillevic, M., Johnsen, S.J., Pedersen, D.S., Popp, T.J., Rasmussen, S.O., Severinghaus, J.P., Svensson, A. and Vinther, B.M., 2014. Consistently dated records from the Greenland GRIP, GISP2 and NGRIP ice cores for the past 104 ka reveal regional millennial-scale delta O-18 gradients with possible Heinrich event imprint. Quaternary Science Reviews, 106: 29-46.

Sejrup, H.P., Fjæran, T., Hald, M., Beck, L., Hagen, J., Miljeteig, I., Morvik, I. and Norvik, O., 1981. Benthonic foraminifera in surface samples from the Norwegian Continental margin between 62°N and 65°N. Journal of Foraminiferal Research, 11(4): 277-295.

Sejrup, H.P., Haflidason, H., Aarseth, I., King, E., Forsberg, C.F., Long, D. and Rokoengen, K., 1994. Late Weichselian Glaciation History of the Northern North-Sea. Boreas, 23(1): 1-13.

Sejrup, H.P., King, E.L., Aarseth, I., Haflidason, H. and Elverhøi, A., 1996. Quaternary erosion and depositional processes: western Norwegian fjords, Norwegian Channel and North Sea Fan. Geological Society, London, Special Publications, 117(1): 187-202.

Sejrup, H.P., Landvik, J.Y., Larsen, E., Janocko, J., Eiriksson, J. and King, E., 1998. The Jæren area, a border zone of the Norwegian channel ice stream. Quaternary Science Reviews, 17(9-10): 801-812.

Sejrup, H.P., Larsen, E., Landvik, J., King, E.L., Haflidason, H. and Nesje, A., 2000. Quaternary glaciations in southern Fennoscandia: evidence from southwestern Norway and the northern North Sea region. Quaternary Science Reviews, 19(7): 667-685.

Sejrup, H.P., Larsen, E., Haflidason, H., Berstad, I.M., Hjelstuen, B.O., Jonsdottir, H.E., King, E.L., Landvik, J., Longva, O., Nygard, A., Ottesen, D., Raunholm, S., Rise, L. and Stalsberg, K., 2003. Configuration, history and impact of the Norwegian Channel Ice Stream. Boreas, 32(1): 18-36.

Sejrup, H.P., Hjelstuen, B.O., Dahlgren, K.I.T., Haflidason, H., Kuijpers, A., Nygard, A., Praeg, D., Stoker, M.S. and Vorren, T.O., 2005. Pleistocene glacial history of the NW European continental margin. Marine and Petroleum Geology, 22(9-10): 1111-1129.

Sejrup, H.P., Nygard, A., Hall, A.M. and Haflidason, H., 2009. Middle and Late Weichselian (Devensian) glaciation history of south-western Norway, North Sea and eastern UK. Quaternary Science Reviews, 28(3-4): 370-380.

Sejrup, H.P., Hjelstuen, B.O., Nygard, A., Haflidason, H. and Mardal, I., 2015. Late Devensian ice-marginal features in the central North Sea processes and chronology. Boreas, 44(1): 1-13.

Sejrup, H.P., Clark, C.D. and Hjelstuen, B.O., 2016. Rapid ice sheet retreat triggered by ice stream debuttressing: Evidence from the North Sea. Geology, 44(5): 355-358.

Stanford, J.D., Rohling, E.J., Bacon, S., Roberts, A.P., Grousset, F.E. and Bolshaw, M., 2011. A new concept for the paleoceanographic evolution of Heinrich event 1 in the North Atlantic. Quaternary Science Reviews, 30(9-10): 1047-1066.

Svendsen, J.I., Briner, J.P., Mangerud, J. and Young, N.E., 2015. Early break-up of the Norwegian Channel Ice Stream during the Last Glacial Maximum. Quaternary Science Reviews, 107: 231-242.

Toucanne, S., Zaragosi, S., Bourillet, J.-F., Marieu, V., Cremer, M., Kageyama, M., Van Vliet-Lanoë, B., Eynaud, F., Turon, J.-L. and Gibbard, P.L., 2010. The first estimation of Fleuve Manche palaeoriver discharge during the last deglaciation: Evidence for Fennoscandian ice sheet meltwater flow in the English Channel ca 20–18ka ago. Earth and Planetary Science Letters, 290(3-4): 459-473.

Toucanne, S., Soulet, G., Freslon, N., Silva Jacinto, R., Dennielou, B., Zaragosi, S., Eynaud, F., Bourillet, J.-F. and Bayon, G., 2015. Millennial-scale fluctuations of the European Ice Sheet at the end of the last glacial, and their potential impact on global climate. Quaternary Science Reviews, 123: 113-133.

Vaughan, D.G. and Arthern, R., 2007. Why Is It Hard to Predict the Future of Ice Sheets? Science, 315: 1503-1504.

Vaughan, D.G., Comiso, J.C., Allison, I., Carrasco, J., Kaser, G., Kwok, R., Mote, P., Murray, T., Paul, F., Ren, J., Rignot, E., Solomina, O., Steffen, K. and Zhang, T., 2013. Observations: Cryosphere. In: T.F. Stocker, D. Qin, G.-K. Plattner, M. Tignor, S.K. Allen, J. Boschung, A. Nauels, Y. Xia, V. Bex and P.M. Midgley (Editors), Climate Change 2013: The Physical Science Basis. Contribution of Working Group I to the Fifth Assessment Report of the Intergovernmental Panel on Climate Change. Cambridge University Press, Cambridge, United Kingdom and New York, NY, USA.

Wary, M., Eynaud, F., Rossignol, L., Lapuyade, J., Gasparotto, M.-C., Londeix, L., Malaizé, B., Castére, M.-H. and Charlier, K., 2016. Norwegian Sea warm pulses during Dansgaard-Oeschger stadials: Zooming in on these anomalies over the 35–41 ka cal BP interval and their impacts on proximal European ice-sheet dynamics. Quaternary Science Reviews, 151: 255-272.

Werner, J.P. and Tingley, M.P., 2015. Technical Note: Probabilistically constraining proxy age–depth models within a Bayesian hierarchical reconstruction model. Climate of the Past, 11(3): 533-545.

Whittington, G. and Edwards, K.J., 1993. Vegetation change on Papa Stour, Shetland, Scotland: a response to coastal evolution and human interference? The Holocene, 3(1): 54-62.

Figure texts

Figure 1: **(A)** The southern Norwegian Sea, red dots indicate studied cores, blue dots reference cores. X1: MD01-2461 (Peck et al., 2006), X2: 300 km north of MD95-2002 (Toucanne et al., 2015). Modern surface currents, the Faroe- (FC), Shetland- (SC), Norwegian Atlantic- (NwAC) and the Norwegian Coastal Current (NCC) are indicated (Hansen and Østerhus, 2000). **(B)** Seabed character of the northern North Sea margin and the Norwegian Channel (NC); bathymetric data from Olex AS. MD99-2284 and MD99-2283 are separated by a submarine bulge. **(C)** A deep-tow boomer profile crossing the >300 m thick North Sea Trough Mouth Fan (NSTMF), position indicated in B. The profile is reproduced with the permission of the British Geological Survey ©NERC. All rights reserved. **(D)** TOPAS high-resolution seismic profile, as indicated in B, demonstrating the position of MD99-2283 relative to the youngest described glacigenic debris flow (GDF). Several layers of sediment are visible below the GDF, which postdate the core top of MD99-2283. **(E)** TOPAS high-resolution seismic profile, as indicated in A, visualizing the stratigraphic position of MD99-2289 relative to the last GDFs. This profile is modified after Reiche et al. (2011).

Figure 2: Individual age models of all cores in this study. The age models are based on 142 accelerator mass spectrometry radiocarbon dates (Table S1) and are computed with the R-based script Bacon (Blaauw and Christen, 2011). The red line marks the weighted mean, the grey shaded area displays the two-sigma uncertainty of each depth in the core. The darker the grey tone, the higher the age model certainty. In core MD99-2283 the Laschamp magnetic reversal was used as an additional age

model constraint. Core MD99-2291 was modelled without the proposed plume event (2.8-15 m core depth). No local reservoir correction was applied.

Figure 3: Results of the analyses of cores MD99-2289, MD99-2283 and MD99-2284 on depth scale. The ∂18O data from Greenland ice core GISP2 are displayed on the GIIC05 time scale, Greenland Interstadials (GIS) and Marine Isotope Stages (MIS) are indicated. Planktonic ∂18O data from the cores is displayed in respect to the VPDB (Vienna Peedee Belemnite) standard. Relative abundances of *N. pachyderma* sin. (Nps) in red, are displayed in light red, if <200 planktonic foraminifera were counted (reversed scale). Grain content is displayed as counts >1 mm per g dry sediment (orange) and counts >150 μm for cores MD83 and MD84 (black). Radiocarbon dated levels (black triangles) and the stratigraphical position of the Faroe Marine Ash Zone (FMAZ) II are indicated. Grey shaded bars indicate tentative correlations between decreases in Nps and Greenland Interstadials. Capital letters D-A denote episodes of increased grain content >150 μm. Numbers in paragraphs within graph captions correspond to the individual references of published data (see Table 2): (x) this study, (1) (Berstad et al., 2003), (2) (Lekens et al., 2006), (3) (Dokken et al., 2013), (4) (Dokken et al., 2015b).

Figure 4: Results of the analyses of core MD99-2289, MD99-2283 and MD99-2284 on individual age model. Coarse grain content is displayed as counts per g dry sediment (orange). Note that the grain size fraction used for counting differs in core MD89 (>1 mm). The grain content in MD84 is additionally given in higher detail in

yellow. Relative abundances of *N. pachyderma* sin. (Nps) in red, are displayed in light red, if <200 planktonic foraminifera were counted (reversed scale). Cumulative grain size values are displayed in their separate fractions. In MD84, fraction 63-150 μm was not subdivided. Radiocarbon dated levels are indicated with black triangles, red triangles denote dates that were removed. Ca/Fe core scanner data are resampled with the nearest point method (Hammer et al., 2001) every 50 years (blue). The ∂18O data from Greenland ice core GISP2 are displayed on the GIIC05 time scale, Greenland Interstadials (GIS) and Marine Isotope Stages (MIS) are indicated. Grey shaded bars indicate tentative correlations between decreases in Nps and Greenland Interstadials. The stratigraphical position of the Faroe Marine Ash Zone (FMAZ) II and the glacigenic debris flows (GDF) 3 and 1 (cf. Fig. 1D and E) are indicated. Capital letters D-A denote episodes of increased grain content >150 μm. Numbers in paragraphs within graph captions correspond to the individual references of published data (see Table 2): (x) this study, (1) (Berstad et al., 2003), (2) (Haflidason et al., 2003), (3) (Lekens et al., 2006), (4) (Dokken et al., 2013), (5) (Dokken et al., 2015b).

Figure 5: Detail of core MD99-2283 between 900-1250 cm core depth, showing that the Ca/Fe counts, carbonates measurements, point measurements of magnetic susceptibility (MS), %Nps (*N. pachyderma* sin. - reversed scale) and coarse grain contents correlate well with the variations in the displayed grain size distribution. Subtle changes in colour mark the change in sediment composition. Radiocarbon dated levels are indicated (black triangles). Tentatively correlated Greenland Interstadials (GIS) are also indicated.

Figure 6: The uppermost three sections of core MD99-2283, subdivided into the identified episodes D to B. Light sediment colour, high Ca/Fe and coarse grain counts, spikes in CaCO3, a high number of small fragments in the X-ray picture and low point measurements of magnetic susceptibility (MS) values mark episode D. Episodes C and B exhibit no sediment colour variation, relatively low and stable Ca/Fe counts, varying, but lower coarse grain counts, occasional pebbles of up to 8 cm in diameter on the X-ray image and high magnetic susceptibility values. %Nps (*N. pachyderma* sin.) shows a distinct warm spike between episodes D and C (reversed scale). Radiocarbon dated levels are indicated (black triangles). Two colour image insets show fraction >1 mm with mollusc fragments >0.5 cm, raster in background is 1 cm.

Figure 7: Linear accumulation rates, calculated between every dated level of all cores. Core MD99-2291 exceeds the scale at around 18.5-19 ka BP. The amount of accumulation varies between 30 cm/ka and up to 350. Two zones of relatively high sedimentation (grey bars) between 35-25.5 ka BP and 22.5-18.5 ka BP are interrupted by periods with lower sedimentation rates.

Figure 8: Compilation of available data from all cores (plotted northeast to southwest), with the relative abundance of Nps (*N. pachyderma* sin.) in red, the content of coarse grains, mainly interpreted as ice rafted debris (IRD), in orange and the isotopic measurements of planktonic ∂18O in black. The isotopic values are reported in respect to the VPDB (Vienna Peedee Belemnite) standard. Note, that the Nps and ∂18O scale is reversed and that the IRD values in MD83 and MD04 are displayed as flux values in [#IRD>150 *µ*m/cm^2/ka]. IRD counting was performed in

the >150 μm fraction, except of MD99-2291 and MD99-2289 (>1 mm). Radiocarbon dated levels are indicated with black triangles, red triangles denote removed dates. The ∂18O data from the Greenland ice core GISP2 are displayed on the GIIC05 time scale, Greenland Interstadials (GIS) and Marine Isotope Stages (MIS) are indicated. Grey shaded bars indicate tentative correlations between decreases in Nps and Greenland Interstadials marked in ∂18O GISP2. The stratigraphical positions of the Faroe Marine Ash Zone (FMAZ) II and the meltwater drainage event (green line) are indicated, FMAZII was not found in MD04 to the authors knowledge. Numbers in paragraphs within graph captions correspond to the individual references of published data (see Table 2): (x) this study, (1) (Dokken and Jansen, 1999), (2) (Berstad et al., 2003), (3) (Lekens et al., 2005), (4) (Lekens et al., 2006), (5) (Rasmussen and Thomsen, 2008), (6) (Scourse et al., 2009), (7) (Dokken et al., 2013), (8) (Dokken et al., 2015a), (9) (Dokken et al., 2015b).

Figure 9: Paleogeographic reconstructions with outlines without new data based on Hughes et al. (2015). The modern flow direction of the Norwegian Atlantic Current (NwAC) indicating warm water inflow (red) and no recorded inflow (orange). Fluvial sediment input (blue arrows) is separated from interpreted ice transport direction (red arrows). Interpreted freshwater pooling and meltwater plume sediments (blue areas) and glaciated areas (white areas) show their inferred extension. LBDC (Ling Bank Drainage Channel); NCIS (Norwegian Channel Ice Stream); FIS (Fennoscandian Ice Sheet); BIIS (British-Irish Ice Sheet).

Figure 10: Episodes (D-A) of increased content of ice rafted debris (IRD) from this study compared to IRD flux off the Irish margin in MD01-2461 (Peck et al., 2006) and riverine influx events (grey bars, R1-R5) observed in Fe/Ca data in the Bay of Biscay in MD95-2002 (Toucanne et al., 2015) and the branched and isoprenoid tetraether (BIT) index (Ménot et al., 2006). See Fig. 1A for the location of MD01-2461 and MD95-2002. North Atlantic IRD episodes are indicated in small letters (d-a) (Bond and Lotti, 1995), North Atlantic Heinrich events in dark grey bars. Note that the age scale of this study was shifted by -1000 years to increase the fit with the data of the other studies on the absolute GIIC05 age scale.

Tables

Table 1: Position, data origin and number of accelerator mass spectrometry radiocarbon dates of the cores used in this study including the individual original data sources.

Table 2: New accelerator mass spectrometry radiocarbon dates for cores MD83, MD84 and MD89 including the identified Faroe Marine Ash Zone (FMAZ) II.

Table 3: Overview of the sampling interval, sieving fractions and original references of the sediment data used in this study.

Supplementary material

Table S1: All accelerator mass spectrometry radiocarbon dates used in this study with the respective original references.

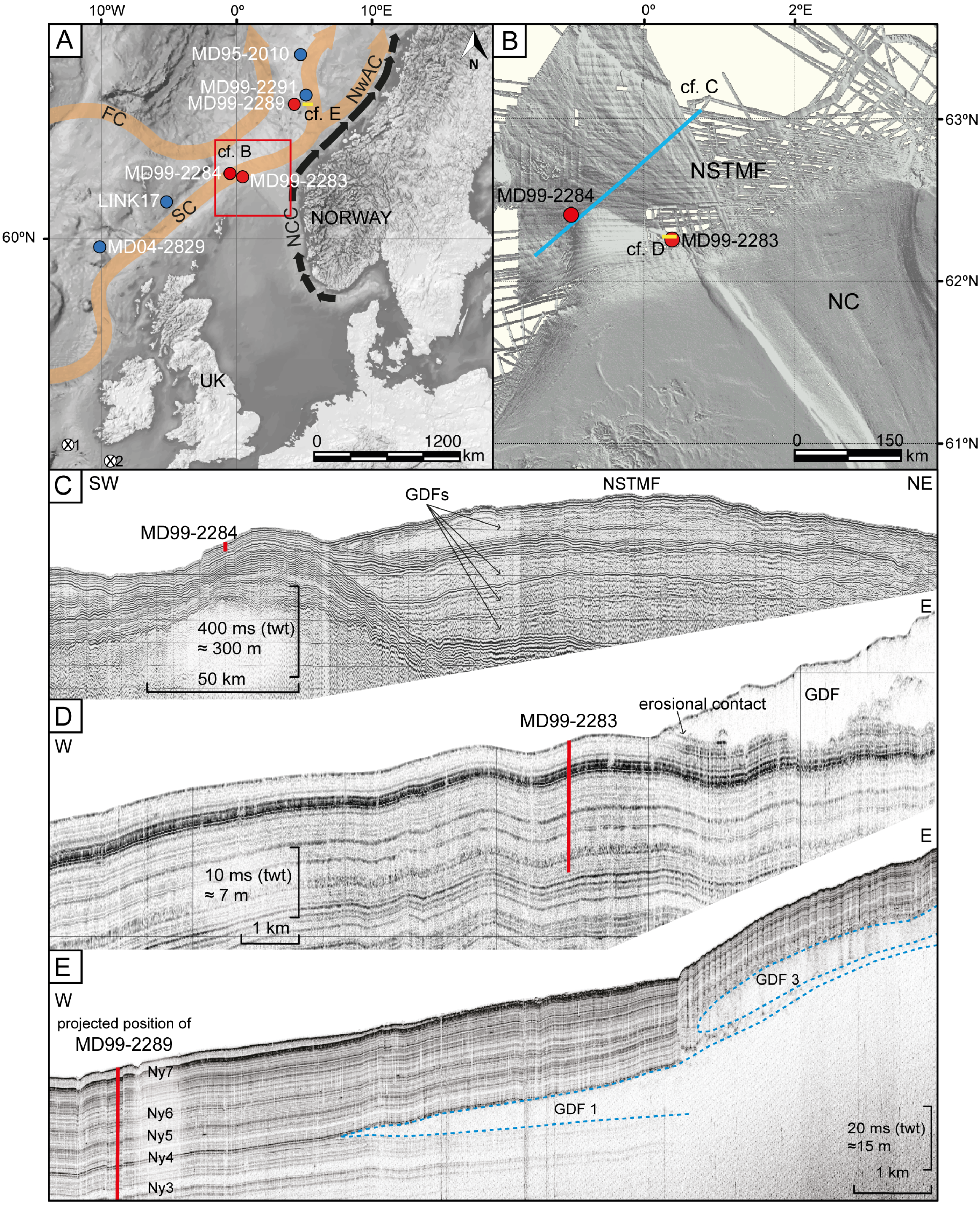

10ºW
0º
10ºE
A
MD95-2010
MD99-2291
MD99-2289
cf. E
FC
NwAC
cf. B
MD99-2284
MD99-2283
LINK17
SC
NCC
NORWAY
60ºN
MD04-2829
UK
1
2
0
1200
km
N
0º
2ºE
B
cf. C
63ºN
NSTMF
MD99-2284
MD99-2283
cf. D
62ºN
NC
0
150
km
61ºN
C
SW
NSTMF
NE
GDFs
MD99-2284
400 ms (twt)
≈ 300 m
50 km
E
D
W
MD99-2283
erosional contact
GDF
10 ms (twt)
≈ 7 m
1 km
E
E
W
projected position of
MD99-2289
GDF 3
Ny7
Ny6
Ny5
Ny4
Ny3
GDF 1
20 ms (twt)
≈15 m
1 km

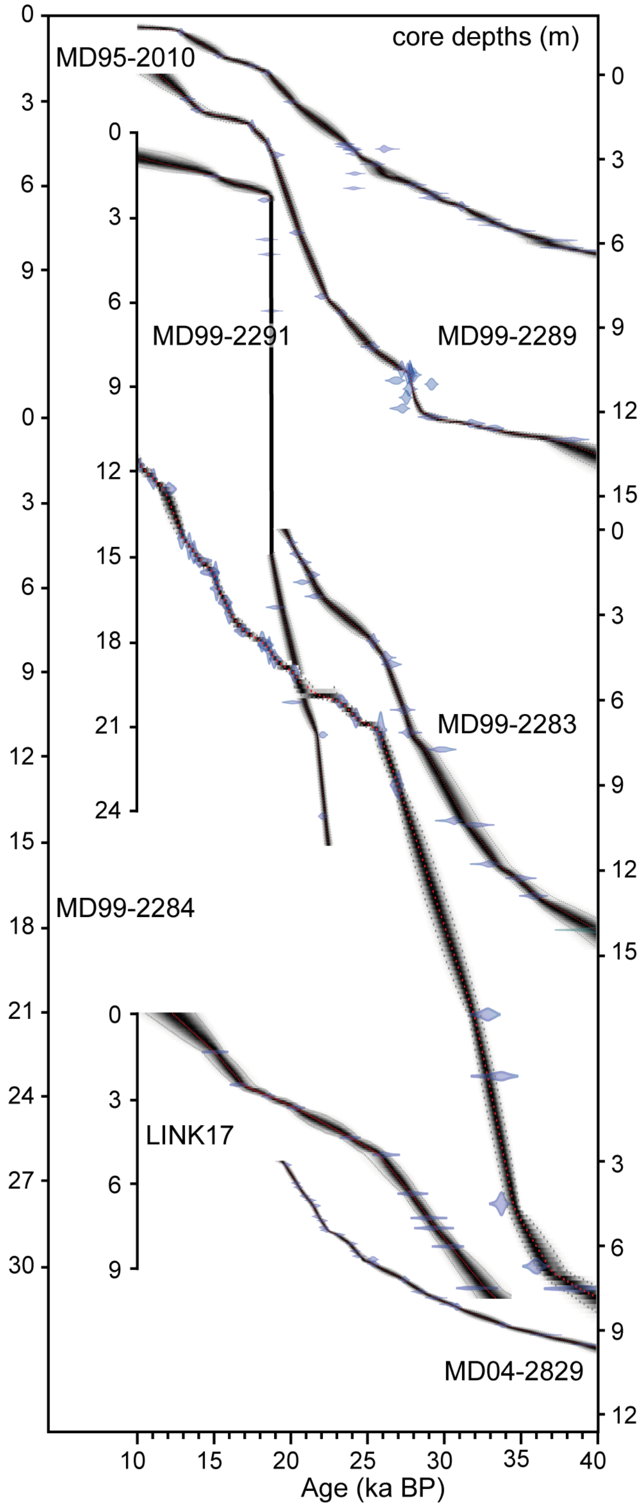

core depths (m)
MD95-2010
MD99-2291
MD99-2289
MD99-2283
MD99-2284
LINK17
MD04-2829
Age (ka BP)

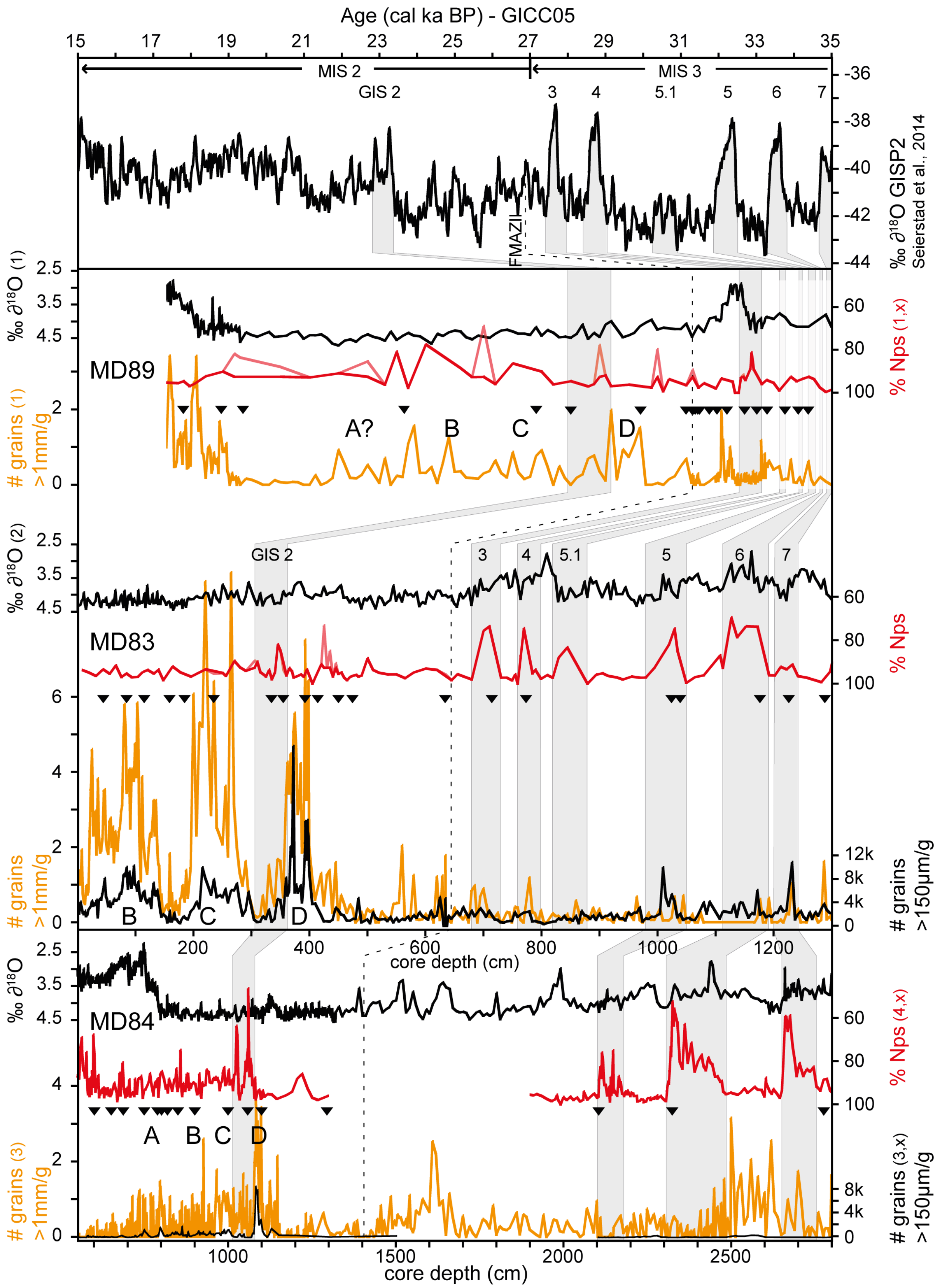

Age (cal ka BP) - GICC05
15 17 19 21 23 25 27 29 31 33 35
MIS 2
MIS 3
GIS 2
3 4 5.1 5 6 7
FMAZII
‰ ∂18O GISP2
Seierstad et al., 2014
-36 -38 -40 -42 -44
MD89
‰ ∂18O (1)
2.5 3.5 4.5
% Nps (1,x)
60 80 100
grains (1) >1mm/g
2 0
A? B C D
MD83
‰ ∂18O (2)
% Nps
6 4 2 0
grains >1mm/g
grains >150µm/g
12k 8k 4k 0
B C D
200 400 600 800 1000 1200
core depth (cm)
MD84
‰ ∂18O
% Nps (4,x)
A B C D
grains (3) >1mm/g
grains (3,x) >150µm/g
8k 4k 0
1000 1500 2000 2500
core depth (cm)

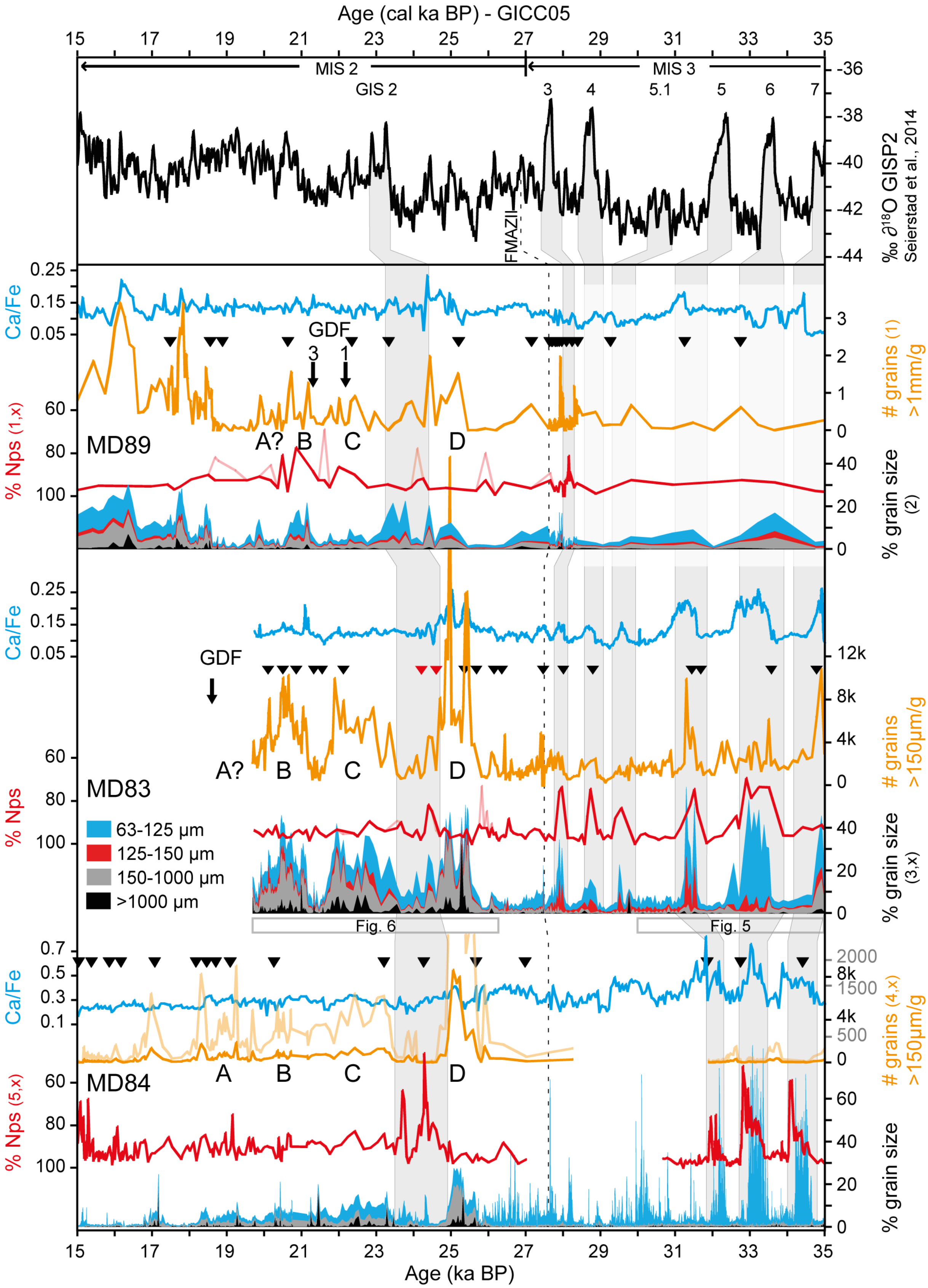

Age (cal ka BP) - GICC05
MIS 2
MIS 3
GIS 2
3
4
5.1
5
6
7
‰ ∂18O GISP2
Seierstad et al., 2014
FMAZII
Ca/Fe
GDF
MD89
A? B C D
% Nps (1,x)
# grains (1) >1mm/g
% grain size (2)
MD83
% Nps
# grains >150µm/g
% grain size (3,x)
63-125 µm
125-150 µm
150-1000 µm
>1000 µm
Fig. 6
Fig. 5
MD84
A B C D
% Nps (5,x)
# grains (4,x) >150µm/g
% grain size
Age (ka BP)

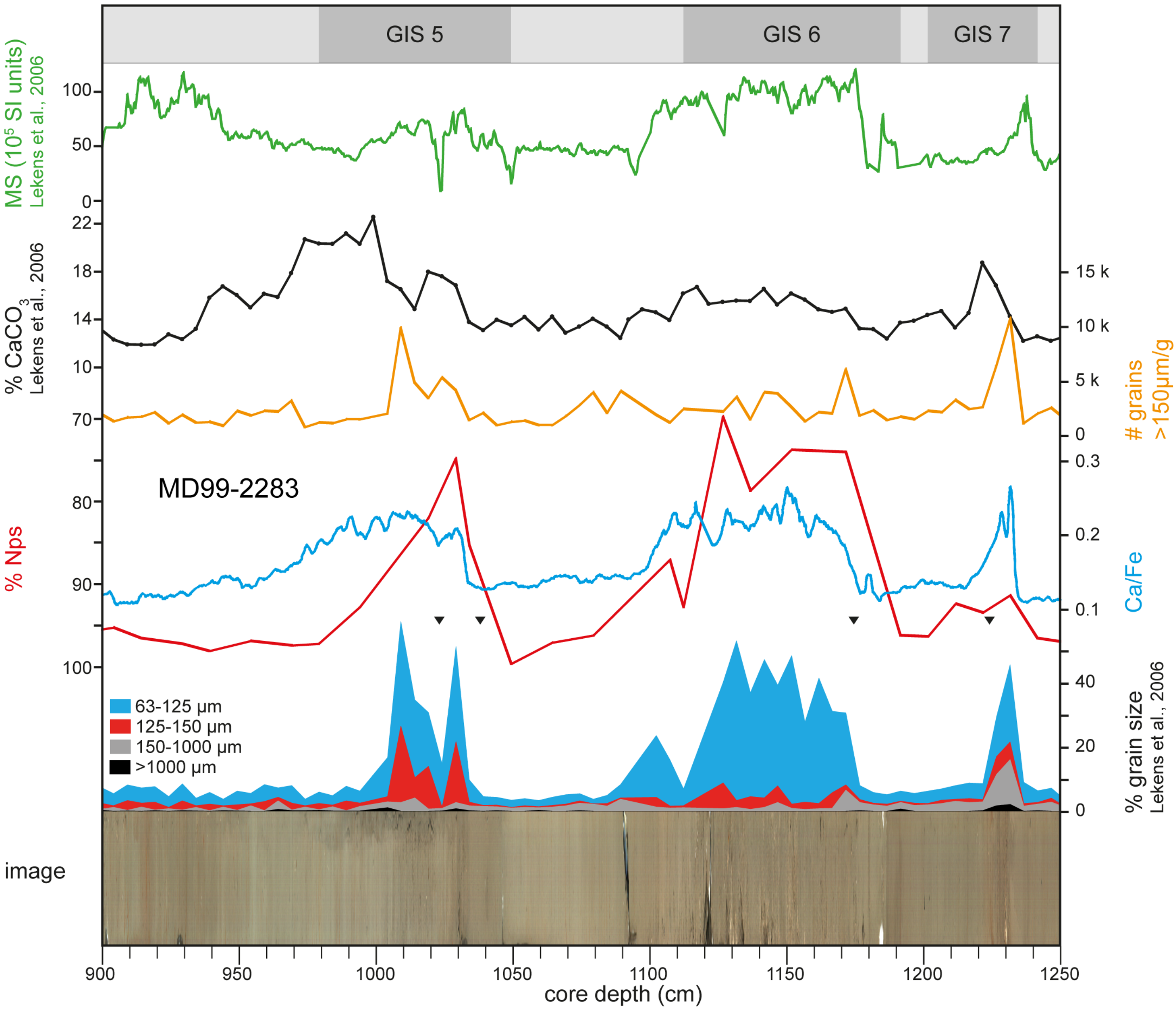

GIS 5
GIS 6
GIS 7
MS (10^5 SI units)
Lekens et al., 2006
100
50
0
22
18
14
10
70
% CaCO$_3$
Lekens et al., 2006
15 k
10 k
5 k
0
grains >150µm/g
80
90
100
% Nps
MD99-2283
0.3
0.2
0.1
Ca/Fe
40
20
0
% grain size
Lekens et al., 2006
63-125 µm
125-150 µm
150-1000 µm
>1000 µm
image
900
950
1000
1050
1100
1150
1200
1250
core depth (cm)

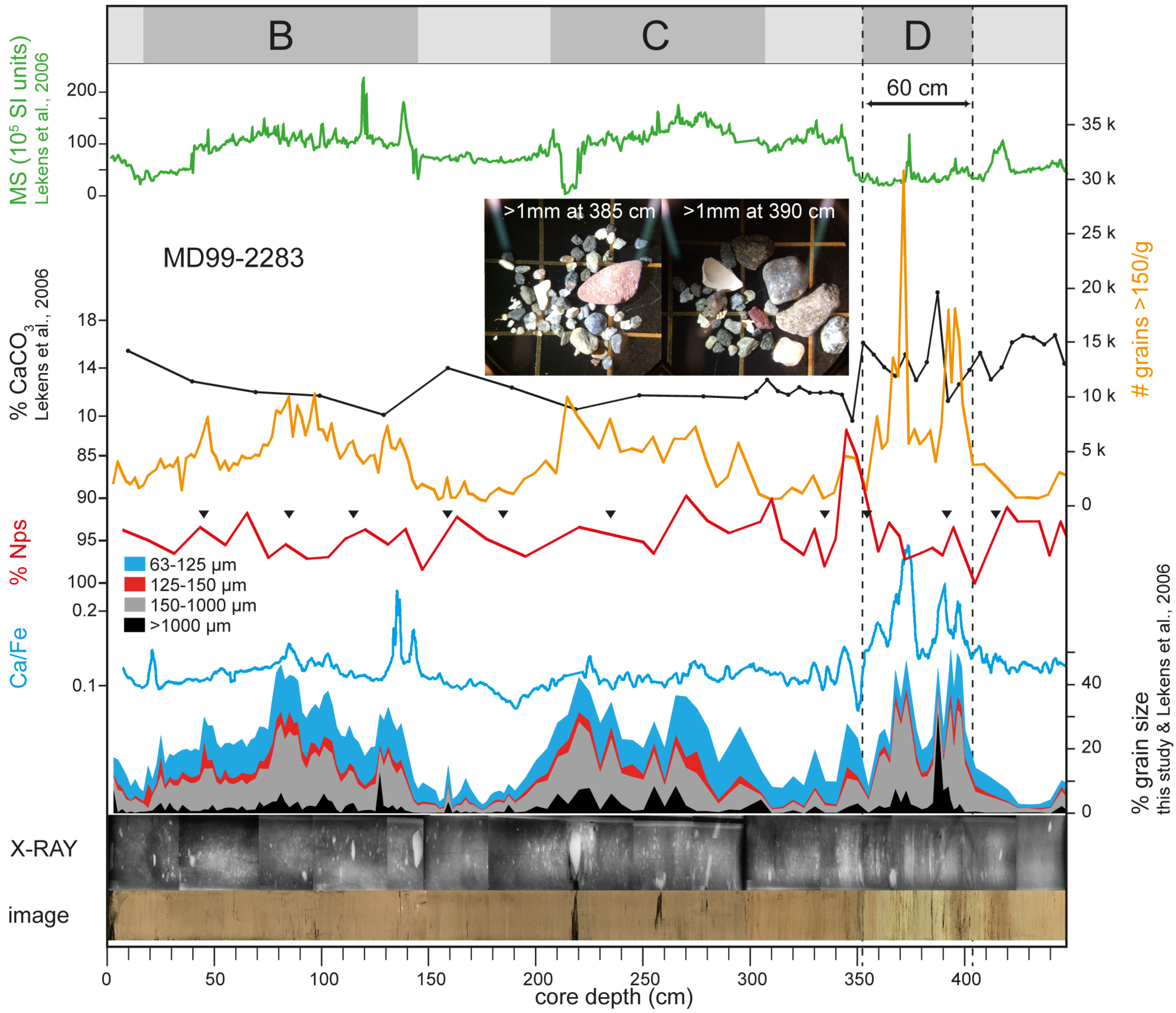

B
C
D
60 cm
MS (10^5 SI units)
Lekens et al., 2006
200
100
0
35 k
30 k
25 k
20 k
15 k
10 k
5 k
0
grains >150/g
MD99-2283
>1mm at 385 cm
>1mm at 390 cm
% CaCO3
Lekens et al., 2006
18
14
10
85
90
95
100
% Nps
63-125 µm
125-150 µm
150-1000 µm
>1000 µm
0.2
0.1
Ca/Fe
40
20
0
% grain size
this study & Lekens et al., 2006
X-RAY
image
0
50
100
150
200
250
300
350
400
core depth (cm)

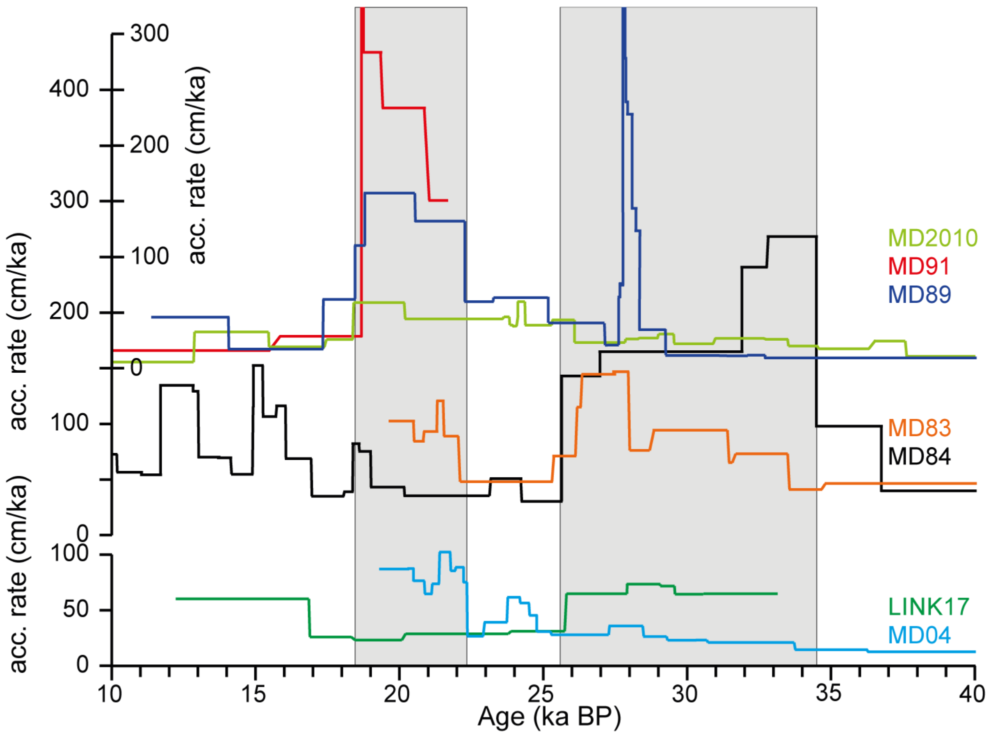
300
200
100
0
acc. rate (cm/ka)
400
300
200
100
0
acc. rate (cm/ka)
100
50
0
acc. rate (cm/ka)
MD2010
MD91
MD89
MD83
MD84
LINK17
MD04
10
15
20
25
30
35
40
Age (ka BP)

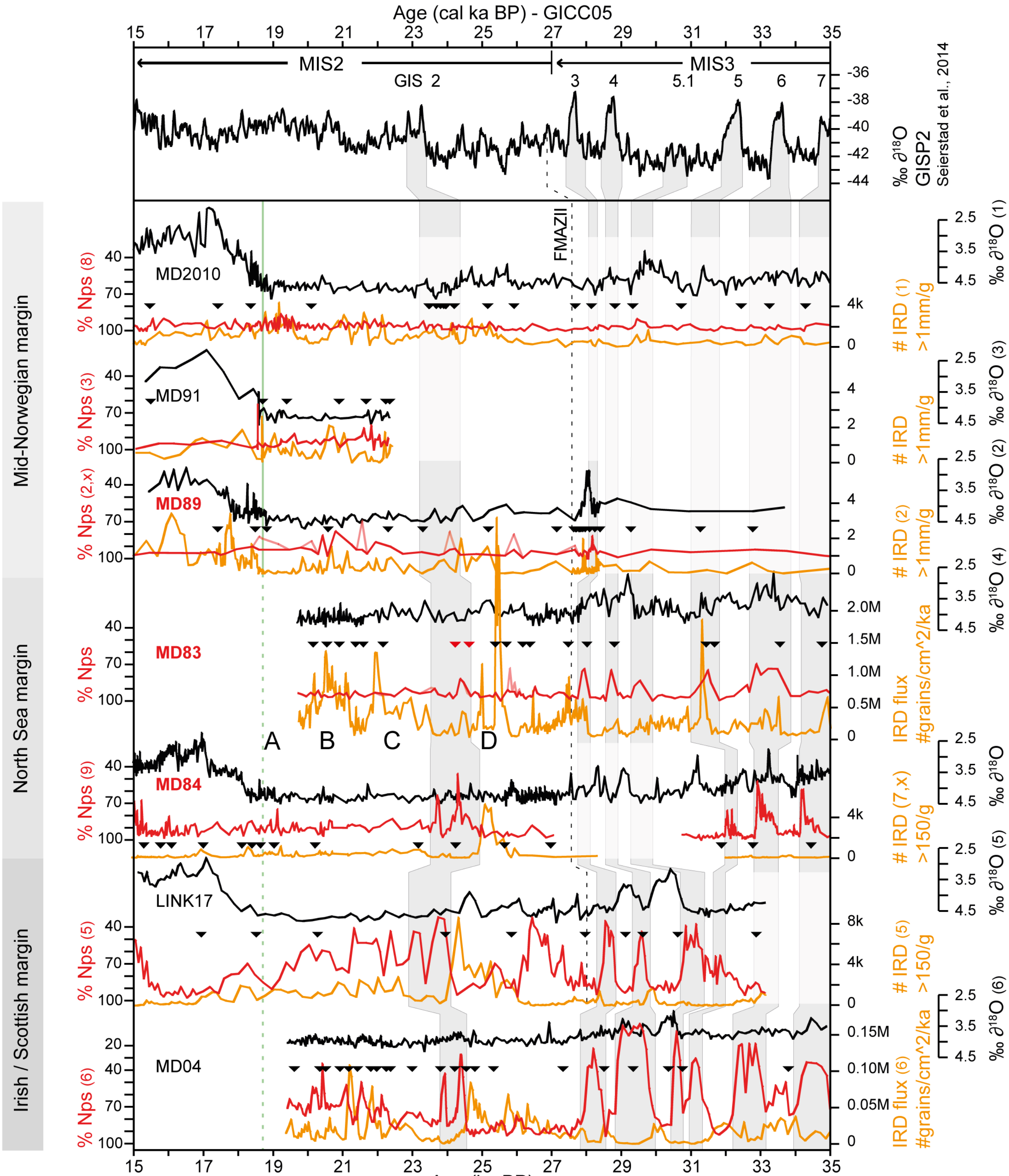

Age (cal ka BP) - GICC05
MIS2
MIS3
GIS 2
3
4
5.1
5
6
7
‰ ∂18O GISP2
Seierstad et al., 2014
FMAZII
Mid-Norwegian margin
North Sea margin
Irish / Scottish margin
MD2010
MD91
MD89
MD83
MD84
LINK17
MD04
% Nps (8)
% Nps (3)
% Nps (2,x)
% Nps
% Nps (9)
% Nps (5)
% Nps (6)
‰ ∂18O (1)
‰ ∂18O (3)
‰ ∂18O (2)
‰ ∂18O (4)
‰ ∂18O
‰ ∂18O (5)
‰ ∂18O (6)
IRD (1) >1mm/g
IRD >1mm/g
IRD (2) >1mm/g
IRD flux #grains/cm^2/ka
IRD (7,x) >150/g
IRD (5) >150/g
IRD flux (6) #grains/cm^2/ka
A
B
C
D
Age (ka BP)

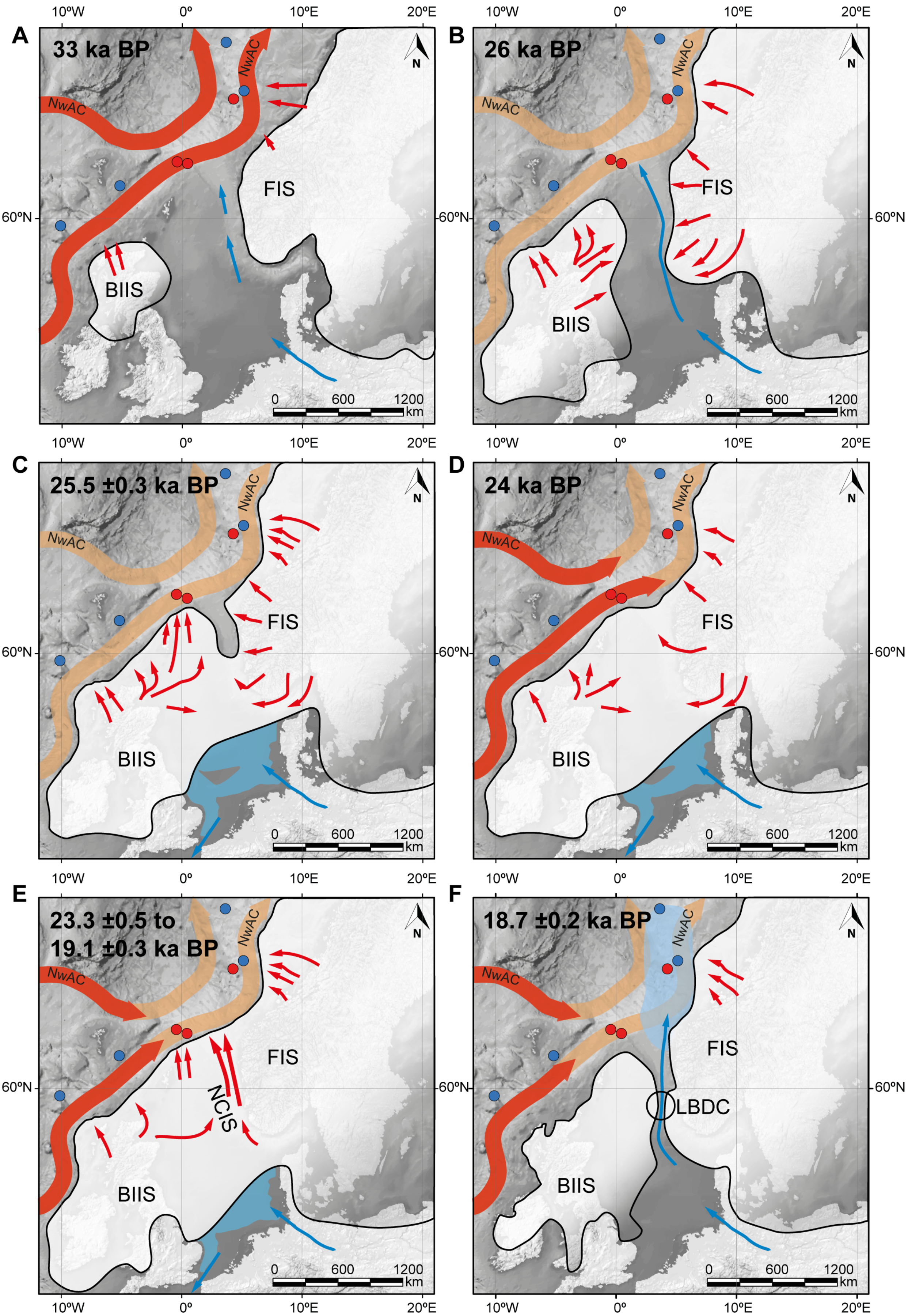
A
33 ka BP
B
26 ka BP
C
25.5 ±0.3 ka BP
D
24 ka BP
E
23.3 ±0.5 to
19.1 ±0.3 ka BP
F
18.7 ±0.2 ka BP
NwAC
FIS
BIIS
NCIS
LBDC
N
10ºW
0º
10ºE
20ºE
60ºN
0
600
1200
km

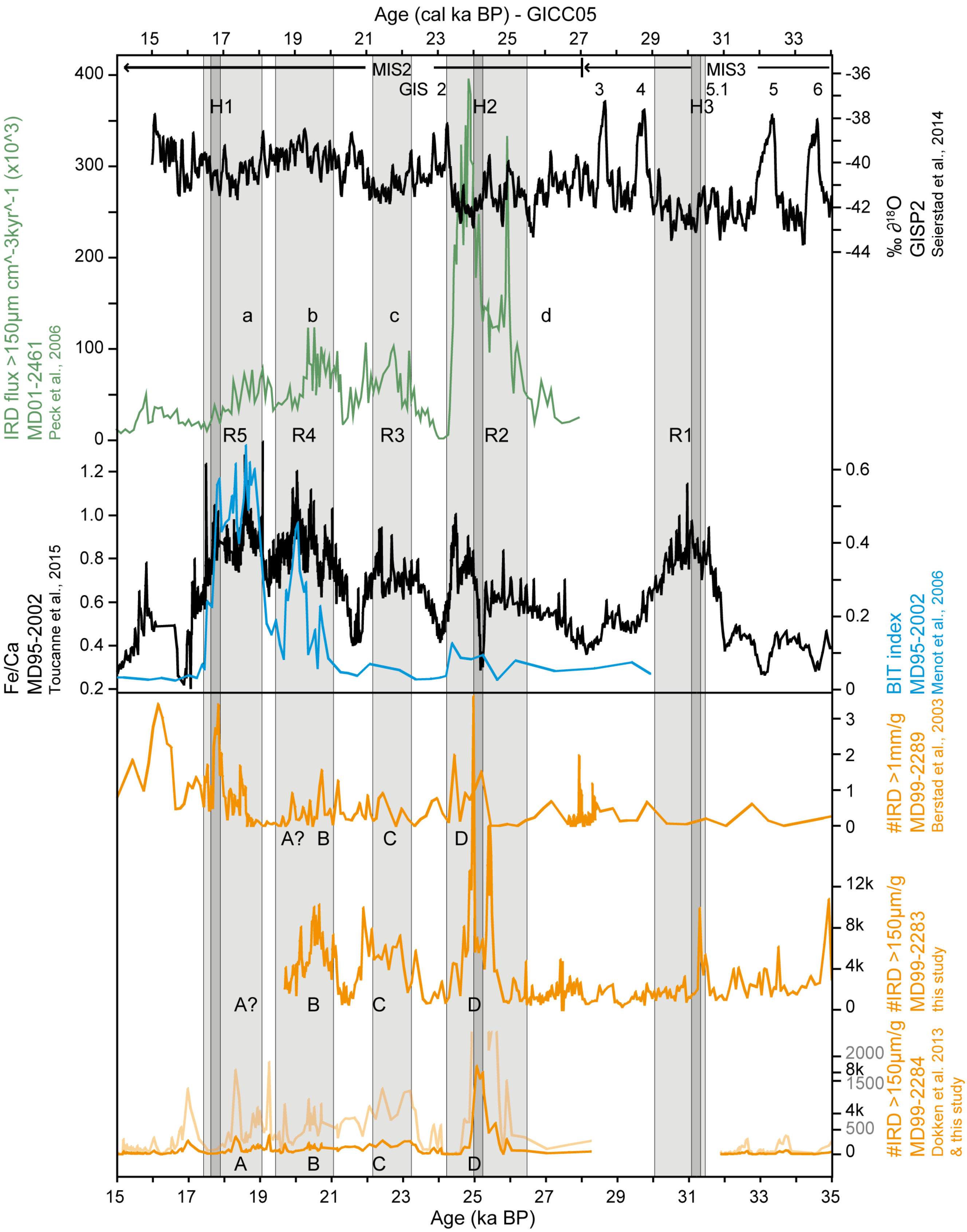

Age (cal ka BP) - GICC05
MIS2
MIS3
GIS 2
3
4
5.1
5
6
H1
H2
H3
a
b
c
d
R5
R4
R3
R2
R1
A? B
C
D
A?
B
C
D
A
B
C
D
IRD flux >150µm cm^-3kyr^-1 (x10^3)
MD01-2461
Peck et al., 2006
‰ ∂18O
GISP2
Seierstad et al., 2014
Fe/Ca
MD95-2002
Toucanne et al., 2015
BIT index
MD95-2002
Menot et al., 2006
#IRD >1mm/g
MD99-2289
Berstad et al., 2003
#IRD >150µm/g
MD99-2283
this study
#IRD >150µm/g
MD99-2284
Dokken et al. 2013
& this study
Age (ka BP)

core	ID	position	water depth [mbsl]	grain size distribution	IRD counts	foraminifera counts	isotope (∂180) sampling	ITRAX data	C14 dating	number of C14 dates	age model	references
MD95-2010	***MD95***	*66.684167°, 4.566160°*	*1226*	-	*(1)*	*(2) & this study*	*(1)*	-	*(1)*	*26*	*this study*	*(1) Dokken et al., 1999; (2) Dokken et al., 2015a*
MD99-2291	***MD91***	*64.938667°, 5.592000°*	*577*	-	*this study*	*(2)*	*(2)*	-	*(1 & 2)*	*12*	*this study*	*(1) Hjelstuen et al., 2004; (2) Lekens et al., 2005*
MD99-2289	**MD89**	64.6680556°, 4.2263889°	1262	(1)	(2)	(2) & this study	(2)	this study	(3) & this study	25	this study	(1) Haflidason et al., 2003; (2) Berstad et al., 2003; (3) Brendryen et al., 2011
MD99-2283	**MD83**	62.261167°, 0.414000°	707	(1) & this study	this study	this study	(1)	this study	(1)	21	this study	(1) Lekens et al., 2006
MD99-2284	**MD84**	62.374667°, -0.980167°	1500	this study	(2) & this study	(3) & this study	this study	this study	(1) & this study	27	this study	(1) Risebrobakken et al., 2011; (2) Dokken et al., 2013; (3) Dokken et al., 2015b
LINK17	***LINK17***	*61.000000°, -5.000000°*	*1500*	-	*(1)*	*(1)*	*(1)*	-	*(1)*	*11*	*this study*	*(1) Rasmussen et al., 2008*
MD04-2829	***MD04***	*58.948830°, -9.571670°*	*1743*	-	*(1)*	*(1)*	*(1)*	-	*(2)*	*24*	*this study*	*(1) Scourse et al., 2009; (2) Hall et al., 2011*

Core	Lab number	depth void corrected (cm)	Material	14C Age uncorrected (ka BP)	absolute age (ka BP)	S.D. 2 σ (ka)	calibrated, modelled age (cal ka BP)	S.D. 2 σ (ka)	∂ absolute and modelled age (ka)	S.D. 2 σ (ka)	reference	Info
MD99-2289	ETH-55533	86.8	Nps	11.782		0.184	13.2451	0.3618			this study	
MD99-2289	Beta 414663	182.0	planktic foraminifera	14.72		0.04	17.3937	0.195			this study	
MD99-2289	Beta 380040	248.8	Nps	15.63		0.05	18.4737	0.1437			this study	
MD99-2289	Beta 380041	850.1	Nps	19.79		0.07	23.2945	0.2784			this study	
MD99-2289	Beta 376421	1049.9	Nps	23.24		0.1	27.1417	0.3678			this study	
MD99-2289	Beta 376422	1059.8	Nps	24.08		0.09	27.6353	0.1656			this study	
MD99-2289	Beta 373227	1062.8	Nps	24.14		0.12	27.682	0.1285			this study	
MD99-2289	FMAZ II	1063.8	tephra		26.69	0.39	27.6951	0.1148	-1.0051	0.287471	Nilsen et al., 2014	not in age model
MD99-2289	Beta 365943	1064.8	Nps	23.83		0.11	27.7083	0.1014			this study	
MD99-2289	Beta 376423	1069.8	Nps	24.4		0.11	27.7754	0.0715			this study	
MD99-2289	Beta 380041	1072.8	Nps	24.2		0.09	27.7882	0.067			this study	
MD99-2289	Beta 380043	1102.8	Nps	25.54		0.11	27.8831	0.0747			this study	
MD99-2289	Beta 380044	1171.8	Nps	27.79		0.13	28.2375	0.2099			this study	reworked - removed
MD99-2289	Beta 380045	1242.8	Nps	28.5		0.14	31.2674	0.8568			this study	
MD99-2283	ETH-72933	334.8	Nps	19.898		0.066	24.18085	0.6677			this study	too young - removed
MD99-2283	BETA-429895	392.3	Nps	21.51		0.07	25.37137	0.2815			this study	
MD99-2283	BETA-429889	449.4	Nps	22.48		0.08	26.14195	0.2272			this study	
MD99-2283	FMAZ II	634.4	tephra		26.69	0.39	27.46892	0.2948	-0.77892	0.345684	this study	not in age model
MD99-2284	Tua-3305	450.5	Nps	11.955		0.09	13.4228	0.1503			this study	
MD99-2284	Tua-3987	472.5	Nps	12.235		0.075	13.7328	0.1662			this study	
MD99-2284	Tua-3988	502.5	Nps	12.595		0.13	14.1728	0.3537			this study	
MD99-2284	Tua-3989	543.5	Nps	12.98		0.13	14.9165	0.2505			this study	
MD99-2284	POZ-10154	546.5	Nps	13.08		0.06	14.942	0.2331			this study	
MD99-2284	KIA-10678	600.5	Nps	13.15		0.07	15.2963	0.215			this study	
MD99-2284	Tua-3306	650.5	Nps	13.55		0.1	15.7671	0.2375			this study	
MD99-2284	POZ-10155	687.5	Nps	13.71		0.06	16.0888	0.1908			this study	
MD99-2284	Tua-3990	749.5	Nps	14.315		0.115	16.9953	0.3516			this study	
MD99-2284	POZ-10156	788.5	Nps	15.33		0.07	18.1126	0.2421			this study	
MD99-2284	Tua-3307	800.5	Nps	15.55		0.19	18.4063	0.2474			this study	
MD99-2284	POZ-10157	819.5	Nps	15.73		0.07	18.6378	0.1723			this study	
MD99-2284	Tua-3991	849.5	Nps	16.105		0.12	19.0389	0.2413			this study	
MD99-2284	Tua-3308	900.5	Nps	17.195		0.09	20.2172	0.2719			this study	
MD99-2284	Tua-3309	1000.5	Nps	19.725		0.12	23.1929	0.3852			this study	
MD99-2284	BETA-429891	1058.5	Nps	20.59		0.08	24.2631	0.2716			this study	
MD99-2284	BETA-429890	1295.5	Nps	23.02		0.08	26.9947	0.3057			this study	
MD99-2284	FMAZ II	1407.5	tephra		26.69	0.39	27.6742	0.4933	-0.9842	0.444632	Dokken et al., 2013	not in age model

Core ID	core depth (m)	sampling interval (cm)	time covered range (a)	average time covered (a)	fractions (µm)	references
MD83	0 - 13	2 - 5	50 - 100	50	<63, 63 - 125, 125 - 150, 150 - 1000 and >1000	Lekens et al. (2006)
	3.5 - 4.5	2.5	10 - 50	50		this study
MD89	1.4 - 13	2-10	10 - 200 (15-25 ka) 200 - 1000 (25-	80		Haflidason et al. (2003)
MD84	5.5 - 30	1	5 - 35	8.7	<63, 63 - 150, 150 - 1000 and	this study

Core	Lab number	depth, void corrected (cm)	Material	14C Age uncorrected (ka BP)	absolute age (ka BP)	S.D. 2 σ (ka)	calibrated, modelled age (cal ka BP)	S.D. 2 σ (ka) (plus)	S.D. 2 σ (ka) (minus)	S.D. 2 σ (ka) (average of both errors)	Original reference	Info
MD95-2010	KIA-6550	9.5	Nps	3.57		0.04	3.00	0.14	0.12	0.13	this study	
MD95-2010	KIA-6551	54.5	Nps	11.42		0.06	12.92	0.17	0.15	0.16	Dokken et al. (1999)	included
MD95-2010	KIA-6552	136.5	Nps	13.25		0.06	15.45	0.26	0.22	0.24	Dokken et al. (1999)	included
MD95-2010	KIA-6553	173.5	Nps	14.75		0.11	17.52	0.32	0.34	0.33	Dokken et al. (1999)	included
MD95-2010	KIA-6554	197.5	Nps	15.62		0.07	18.50	0.19	0.23	0.21	Dokken et al. (1999)	included
MD95-2010	KIA-6555	300.5	Nps	16.99		0.11	20.17	0.30	0.31	0.31	Dokken et al. (1999)	included
MD95-2010	GifA-96476	449.5	Nps	19.83		0.13	23.61	0.23	0.27	0.25	Dokken et al. (1999)	included
MD95-2010	GifA-96477	450.5	Nps	20.03		0.11	23.63	0.23	0.27	0.25	Dokken et al. (1999)	included
MD95-2010	GifA-96487	459.5	Nps	19.93		0.12	23.79	0.24	0.25	0.25	Dokken et al. (1999)	included
MD95-2010	GifA-96489	464.5	Nps	20.34		0.12	24.05	0.15	0.16	0.15	Dokken et al. (1999)	included
MD95-2010	GifA-96683	467.5	Nps	22.26		0.18	24.21	0.14	0.14	0.14	Dokken et al. (1999)	included
MD95-2010	GifA-96490	469.5	Nps	20.34		0.13	24.32	0.17	0.17	0.17	Dokken et al. (1999)	included
MD95-2010	GifA-96684	470.5	Nps	20.39		0.16	24.35	0.18	0.18	0.18	Dokken et al. (1999)	included
MD95-2010	GifA-96492	484.5	Nps	20.45		0.12	24.45	0.17	0.17	0.17	Dokken et al. (1999)	included
MD95-2010	GifA-96685	521.5	Nps	21.59		0.19	24.84	0.30	0.21	0.25	Dokken et al. (1999)	included
MD95-2010	KIA-6556	554.5	Nps	20.49		0.14	25.13	0.26	0.23	0.25	Dokken et al. (1999)	included
MD95-2010	GifA-96686	594.5	Nps	24.33		0.22	26.09	0.51	0.20	0.36	Dokken et al. (1999)	included
MD95-2010	GifA-96491	606.5	Nps	20.42		0.17	26.16	0.55	0.19	0.37	Dokken et al. (1999)	included
MD95-2010	GifA-96493	624.5	Nps	25.54		0.20	27.96	0.64	0.39	0.52	Dokken et al. (1999)	included
MD95-2010	KIA-6557	640.5	Nps	25.52		0.24	29.63	0.54	0.43	0.49	Dokken et al. (1999)	included
MD95-2010	GifA-96496	670.5	Nps	27.45		0.20	31.05	0.33	0.44	0.39	Dokken et al. (1999)	included
MD95-2010	GifA-96497	716.5	Nps	28.94		0.24	32.74	0.56	0.59	0.58	Dokken et al. (1999)	included
MD95-2010	GifA-96687	737.0	Nps	29.67		0.26	33.55	0.42	0.51	0.47	Dokken et al. (1999)	included
MD95-2010	GifA-96688	757.5	Nps	31.24		0.30	34.67	0.55	0.54	0.55	Dokken et al. (1999)	included
MD95-2010	GifA-96494	790.5	Nps	33.42		0.37	36.70	0.70	0.71	0.70	Dokken et al. (1999)	included
MD95-2010	GifA-96689	816.5	Nps	33.82		0.39	37.76	0.75	0.82	0.79	Dokken et al. (1999)	included
MD95-2010	GifA-96690	827.5	Nps	35.48		0.55	38.89	0.78	0.79	0.79	Dokken et al. (1999)	included
MD95-2010	KIA-6558	861.5	Nps	38.56		0.91	42.06	1.39	1.44	1.41	Dokken et al. (1999)	
MD95-2010	KIA-6559	903.5	Nps	45.94		2.46	46.75	3.33	2.58	2.96	Dokken et al. (1999)	
MD99-2291	KIA-18160	10.0	Npd	15.86		0.10	4.06	0.92	1.14	1.03	Lekens et al. (2005)	reworked
MD99-2291	ETH-257121	16.5	Nps and Npd	4.24		0.28	4.48	0.76	0.75	0.75	Lekens et al. (2005)	
MD99-2291	KIA-19317	60.8	N. labradorica	13.02		0.07	7.28	2.53	2.14	2.34	Lekens et al. (2005)	reworked
MD99-2291	ETH-25488	100.0	benthic foraminifera	10.74		0.17	9.23	2.84	2.64	2.74	Lekens et al. (2005)	
MD99-2291	ETH-25495	180.0	benthic foraminifera	13.05		0.11	15.48	1.20	0.95	1.08	Lekens et al. (2005)	included
MD99-2291	ETH-25958	280.0	benthic foraminifera	15.40		0.14	18.69	0.22	0.25	0.23	Lekens et al. (2005)	included
MD99-2291	Poz-3950	367.0	Yoldiella lenticula	16.12		0.07	18.69	0.20	0.20	0.20	Lekens et al. (2005)	included
MD99-2291	Poz-3951	455.0	Yoldiella lenticula	16.11		0.07	18.70	0.20	0.20	0.20	Lekens et al. (2005)	included
MD99-2291	Poz-3952	614.5	Yoldiella lenticula	16.20		0.06	18.70	0.20	0.20	0.20	Lekens et al. (2005)	included
MD99-2291	ETH-22959	1690.0	Nps	16.10		0.25	19.39	0.31	0.32	0.32	Lekens et al. (2005)	included
MD99-2291	ETH-22960	2040.0	Nps	17.05		0.25	20.88	0.38	0.40	0.39	Lekens et al. (2005)	included
MD99-2291	Poz-3956	2168.0	Yoldiella lenticula	18.62		0.08	21.66	0.24	0.32	0.28	Lekens et al. (2005)	included
MD99-2291	Poz-3957	2375.0	Yoldiella lenticula	18.61		0.08	22.23	0.20	0.21	0.21	Lekens et al. (2005)	included
MD99-2291	ETH-22961	2523.0	Nps	16.63		0.25	22.35	0.21	0.22	0.21	Lekens et al. (2005)	included
MD99-2289	ETH-55533	86.8	Nps	11.78		0.18	13.25	0.35	0.37	0.36	this study	included
MD99-2289	AAR-6234	124.5	Nps	12.41		0.14	14.07	0.59	0.36	0.48	Reiche et al. (2011)	included
MD99-2289	Beta-414663	182.0	planktic foraminifera	14.72		0.04	17.39	0.18	0.21	0.19	this study	included
MD99-2289	Beta-380040	248.8	Nps	15.63		0.05	18.47	0.14	0.14	0.14	this study	included
MD99-2289	AAR-6235	285.8	planktic foraminifera	16.16		0.17	18.81	0.22	0.21	0.21	Reiche et al. (2011)	included
MD99-2289	AAR-6236	563.2	Nps	17.31		0.16	20.57	0.31	0.31	0.31	Reiche et al. (2011)	included
MD99-2289	ETH-25496	790.1	Nps	18.56		0.13	22.29	0.20	0.26	0.23	Reiche et al. (2011)	included
MD99-2289	Beta-380041	850.1	Nps	19.79		0.07	23.29	0.27	0.29	0.28	this study	included
MD99-2289	ETH-25497	969.8	Nps	21.37		0.16	25.18	0.39	0.49	0.44	Reiche et al. (2011)	included
MD99-2289	Beta-376421	1049.9	Nps	23.24		0.10	27.14	0.34	0.40	0.37	this study	included
MD99-2289	Beta-376422	1059.8	Nps	24.08		0.09	27.64	0.13	0.20	0.17	this study	included
MD99-2289	Beta-373227	1062.8	Nps	24.14		0.12	27.68	0.11	0.15	0.13	this study	included
MD99-2289	Beta-365943	1064.8	Nps	23.83		0.11	27.71	0.09	0.11	0.10	this study	included
MD99-2289	Beta-376423	1069.8	Nps	24.40		0.11	27.78	0.07	0.07	0.07	this study	included
MD99-2289	Beta-380041	1072.8	Nps	24.20		0.09	27.79	0.07	0.07	0.07	this study	included
MD99-2289	ETH-23313	1089.8	Nps	22.95		0.20	27.84	0.07	0.07	0.07	Reiche et al. (2011)	included
MD99-2289	Beta-380043	1102.8	Nps	25.54		0.11	27.88	0.09	0.06	0.07	this study	included
MD99-2289	ETH-25498	1119.8	Nps	23.99		0.20	27.95	0.14	0.09	0.11	Reiche et al. (2011)	included
MD99-2289	ETH-23314	1150.3	Nps	23.69		0.20	28.09	0.19	0.14	0.17	Reiche et al. (2011)	included
MD99-2289	Beta-380044	1171.8	Nps	27.79		0.13	28.24	0.23	0.19	0.21	this study	reworked
MD99-2289	ETH-25499	1189.3	Nps	23.32		0.24	28.38	0.24	0.24	0.24	Reiche et al. (2011)	included
MD99-2289	ETH-23315	1219.8	Nps	25.46		0.32	29.26	0.75	0.60	0.68	Reiche et al. (2011)	included

MD99-2289	Beta-380045	1242.8	Nps	28.50		0.14	31.27	0.84	0.88	0.86	this study	included
MD99-2289	ETH-24870	1259.8	Nps	29.42		0.27	32.77	0.74	0.75	0.75	Reiche et al. (2011)	included
MD99-2289	ETH-24871	1299.8	Nps	34.25		0.43	37.01	1.35	1.30	1.32	Reiche et al. (2011)	included
MD99-2283	Poz-3945	45.0	Nps	17.08		0.07	20.12	0.23	0.24	0.23	Lekens et al. (2006)	included
MD99-2283	Poz-3946	85.0	Nps	17.36		0.07	20.51	0.20	0.20	0.20	Lekens et al. (2006)	included
MD99-2283	Poz-3947	115.0	Nps	17.75		0.08	20.86	0.23	0.22	0.22	Lekens et al. (2006)	included
MD99-2283	Poz-3948	159.0	Nps	18.19		0.08	21.34	0.29	0.31	0.30	Lekens et al. (2006)	included
MD99-2283	ETH-26404	185.0	Nps	17.68		0.14	21.55	0.34	0.34	0.34	Lekens et al. (2006)	included
MD99-2283	ETH-24515	235.0	Nps	18.28		0.13	22.11	0.46	0.42	0.44	Lekens et al. (2006)	included
MD99-2283	ETH-72933	334.8	Nps	19.90		0.07	24.18	0.62	0.71	0.67	this study	too young
MD99-2283	ETH-26405	354.8	Nps	19.74		0.15	24.60	0.53	0.66	0.60	Lekens et al. (2006)	too young
MD99-2283	BETA-429895	392.3	Nps	21.51		0.07	25.37	0.25	0.31	0.28	this study	included
MD99-2283	ETH-24514	414.8	Nps	20.87		0.18	25.69	0.29	0.32	0.30	Lekens et al. (2006)	included
MD99-2283	BETA-429889	449.4	Nps	22.48		0.08	26.14	0.22	0.23	0.23	this study	included
MD99-2283	Poz-7179	474.4	Nps	22.74		0.12	26.36	0.24	0.24	0.24	Lekens et al. (2006)	included
MD99-2283	ETH-26406	634.4	Nps	23.67		0.22	27.47	0.29	0.30	0.29	Lekens et al. (2006)	included
MD99-2283	ETH-24513	714.4	Nps	24.03		0.21	28.01	0.44	0.35	0.39	Lekens et al. (2006)	included
MD99-2283	ETH-24512	773.7	Nps	26.13		0.22	28.80	0.63	0.56	0.60	Lekens et al. (2006)	included
MD99-2283	ETH-24511	1024.3	Nps	26.82		0.25	31.46	0.88	0.62	0.75	Lekens et al. (2006)	included
MD99-2283	Poz-7180	1039.3	Nps	28.60		0.26	31.69	0.82	0.58	0.70	Lekens et al. (2006)	included
MD99-2283	Poz-3953	1176.9	Nps	29.24		0.18	33.57	0.74	0.55	0.65	Lekens et al. (2006)	included
MD99-2283	ETH-24516	1226.9	Gastropode	31.52		0.28	34.79	0.56	0.57	0.56	Lekens et al. (2006)	included
MD99-2283	Poz-3954	1288.9	Bivalve	32.44		0.23	36.13	0.91	0.59	0.75	Lekens et al. (2006)	included
MD99-2283	Laschamp	1408.9	magnetic reversal		40.65	0.95	39.98	1.39	1.30	1.34	Lekens et al. (2006)	included
MD99-2284	KIA-10676	2.5	Nps	1.69		0.03	1.32	0.06	0.07	0.07	Risebrobakken et al. (2014)	
MD99-2284	Poz-10150	19.5	Nps	3.52		0.04	3.46	0.10	0.11	0.10	Risebrobakken et al. (2014)	
MD99-2284	Poz-10151	36.5	Nps	5.30		0.04	5.75	0.14	0.09	0.11	Risebrobakken et al. (2014)	
MD99-2284	Poz-10157	53.5	Nps	7.30		0.04	7.75	0.08	0.08	0.08	Risebrobakken et al. (2014)	
MD99-2284	Poz-33098	71.5	Nps	7.94		0.07	8.55	0.15	0.12	0.13	Risebrobakken et al. (2014)	
MD99-2284	TUa-3301	100.5	Nps	8.68		0.09	9.32	0.18	0.23	0.21	Risebrobakken et al. (2014)	
MD99-2284	Poz-33098	165.5	Nps	9.34		0.09	10.22	0.24	0.26	0.25	Risebrobakken et al. (2014)	included
MD99-2284	TUa-3302	213.5	Nps	10.05		0.10	11.07	0.19	0.25	0.22	Risebrobakken et al. (2014)	included
MD99-2284	TUa-3304	249.5	Nps	10.70		0.09	11.73	0.39	0.34	0.37	Risebrobakken et al. (2014)	included
MD99-2284	Poz-29526	423.5	Nps	11.44		0.08	13.04	0.18	0.21	0.19	Risebrobakken et al. (2014)	included
MD99-2284	Tua-3305	450.5	Nps	11.96		0.09	13.42	0.16	0.14	0.15	this study	included
MD99-2284	Tua-3987	472.5	Nps	12.24		0.08	13.73	0.16	0.17	0.17	this study	included
MD99-2284	Tua-3988	502.5	Nps	12.60		0.13	14.17	0.42	0.28	0.35	this study	included
MD99-2284	Tua-3989	543.5	Nps	12.98		0.13	14.92	0.24	0.26	0.25	this study	included
MD99-2284	POZ-10154	546.5	Nps	13.08		0.06	14.94	0.23	0.24	0.23	this study	included
MD99-2284	KIA-10678	600.5	Nps	13.15		0.07	15.30	0.24	0.19	0.22	this study	included
MD99-2284	Tua-3306	650.5	Nps	13.55		0.10	15.77	0.23	0.25	0.24	this study	included
MD99-2284	POZ-10155	687.5	Nps	13.71		0.06	16.09	0.18	0.20	0.19	this study	included
MD99-2284	Tua-3990	749.5	Nps	14.32		0.12	17.00	0.36	0.34	0.35	this study	included
MD99-2284	POZ-10156	788.5	Nps	15.33		0.07	18.11	0.24	0.25	0.24	this study	included
MD99-2284	Tua-3307	800.5	Nps	15.55		0.19	18.41	0.24	0.26	0.25	this study	included
MD99-2284	POZ-10157	819.5	Nps	15.73		0.07	18.64	0.16	0.19	0.17	this study	included
MD99-2284	Tua-3991	849.5	Nps	16.11		0.12	19.04	0.27	0.21	0.24	this study	included
MD99-2284	Tua-3308	900.5	Nps	17.20		0.09	20.22	0.27	0.27	0.27	this study	included
MD99-2284	Tua-3309	1000.5	Nps	19.73		0.12	23.19	0.38	0.39	0.39	this study	included
MD99-2284	BETA-429891	1058.5	Nps	20.59		0.08	24.26	0.26	0.28	0.27	this study	included
MD99-2284	TUa-3310	1100.5	Nps	21.98		0.16	25.67	0.32	0.38	0.35	Dokken et al. (2013)	included
MD99-2284	BETA-429890	1295.5	Nps	23.02		0.08	26.99	0.30	0.32	0.31	this study	included
MD99-2284	POZ-29522	2106.5	Nps	29.10		0.24	31.91	0.45	0.38	0.41	Dokken et al. (2013)	included
MD99-2284	POZ-29523	2324.5	Nps	29.90		0.60	32.82	0.49	0.48	0.48	Dokken et al. (2013)	included
MD99-2284	POZ-17620	2775.5	Nps	29.92		0.24	34.50	0.36	0.46	0.41	Dokken et al. (2013)	included
MD99-2284	POZ-17621	2996.5	Nps	32.50		0.30	36.77	0.97	0.81	0.89	Dokken et al. (2013)	included
MD99-2284	POZ-29524	3075.5	Nps	34.60		0.70	38.81	1.26	1.23	1.25	Dokken et al. (2013)	included
LINK17	AAR-7236	135.0	Nps	13.16		0.15	15.00	0.64	0.80	0.72	Rasmussen et al. (2008)	included
LINK17	AAR-7237	250.0	Nps	14.12		0.12	16.93	0.69	0.54	0.61	Rasmussen et al. (2008)	included
LINK17	AAR-8137	290.0	Nps	15.73		0.11	18.52	0.35	0.43	0.39	Rasmussen et al. (2008)	included
LINK17	AAR-7238	331.0	Nps	17.28		0.14	20.27	0.51	0.56	0.53	Rasmussen et al. (2008)	included
LINK17	AAR-7239	436.5	Bivalve	20.33		0.19	23.93	0.63	0.69	0.66	Rasmussen et al. (2008)	included
LINK17	AAR-8138	496.5	Nps	22.30		0.22	25.85	0.58	0.94	0.76	Rasmussen et al. (2008)	included
LINK17	AAR-7240	633.0	Nps	24.25		0.35	27.95	0.56	0.59	0.57	Rasmussen et al. (2008)	included
LINK17	AAR-8139	718.5	Nps	25.35		0.30	29.11	0.54	0.54	0.54	Rasmussen et al. (2008)	included
LINK17	AAR-8140	754.0	Nps	25.65		0.35	29.61	0.59	0.54	0.56	Rasmussen et al. (2008)	included
LINK17	AAR-8141	818.5	Nps	26.85		0.35	30.61	0.55	0.68	0.62	Rasmussen et al. (2008)	included
LINK17	AAR-8142	965.0	Nps	28.45		0.45	32.87	1.02	0.99	1.01	Rasmussen et al. (2008)	included
MD04-2829	SUERC-8793	312.5	Nps	16.73		0.07	19.60	0.17	0.16	0.16	Hall et al. (2011)	included
MD04-2829	SUERC-8794	376.5	Nps	17.25		0.07	20.33	0.15	0.16	0.16	Hall et al. (2011)	included

MD04-2829	SUERC-8795	391.5	Nps	17.38		0.07	20.51	0.14	0.15	0.15	Hall et al. (2011)	included
MD04-2829	SUERC-8797	422.5	Nps	17.71		0.07	20.91	0.16	0.16	0.16	Hall et al. (2011)	included
MD04-2829	SUERC-8798	438.5	Nps	17.99		0.08	21.16	0.17	0.16	0.16	Hall et al. (2011)	included
MD04-2829	SUERC-8799	457.5	Nps	18.23		0.08	21.42	0.16	0.17	0.16	Hall et al. (2011)	included
MD04-2829	SUERC-8802	495.5	Nps	18.31		0.08	21.79	0.14	0.15	0.15	Hall et al. (2011)	included
MD04-2829	SUERC-8803	510.5	Nps	18.57		0.08	21.97	0.15	0.14	0.15	Hall et al. (2011)	included
MD04-2829	SUERC-8804	534.5	Nps	18.67		0.08	22.24	0.13	0.14	0.14	Hall et al. (2011)	included
MD04-2829	SUERC-8805	544.5	Nps	18.80		0.08	22.37	0.12	0.13	0.12	Hall et al. (2011)	included
MD04-2829	SUERC-8807	560.5	Nps	19.60		0.09	22.98	0.26	0.25	0.25	Hall et al. (2011)	included
MD04-2829	SUERC-8808	592.5	Nps	20.33		0.10	23.79	0.22	0.23	0.23	Hall et al. (2011)	included
MD04-2829	SUERC-8809	618.5	Nps	20.51		0.10	24.21	0.21	0.20	0.20	Hall et al. (2011)	included
MD04-2829	SUERC-8812	636.5	Nps	20.70		0.11	24.54	0.31	0.22	0.26	Hall et al. (2011)	included
MD04-2829	SUERC-8813	648.5	Nps	21.38		0.12	24.79	0.36	0.23	0.30	Hall et al. (2011)	included
MD04-2829	SUERC-8814	664.5	Nps	21.45		0.12	25.31	0.26	0.27	0.27	Hall et al. (2011)	included
MD04-2829	SUERC-8815	720.5	Nps	23.51		0.15	27.32	0.27	0.30	0.29	Hall et al. (2011)	included
MD04-2829	SUERC-8816	762.5	Nps	24.78		0.17	28.50	0.29	0.33	0.31	Hall et al. (2011)	included
MD04-2829	SUERC-8817	784.5	G. bulloides	25.71		0.20	29.34	0.38	0.39	0.38	Hall et al. (2011)	included
MD04-2829	SUERC-1090	807.5	Nps	26.48		0.15	30.35	0.31	0.38	0.35	Hall et al. (2011)	included
MD04-2829	SUERC-1089	816.5	Nps	26.96		0.15	30.74	0.25	0.29	0.27	Hall et al. (2011)	included
MD04-2829	SUERC-1090	880.5	Nps	30.07		0.22	33.79	0.43	0.48	0.45	Hall et al. (2011)	included
MD04-2829	SUERC-1090	916.5	Nps	32.91		0.31	36.33	0.81	0.70	0.75	Hall et al. (2011)	included
MD04-2829	SUERC-1090	950.5	Nps	35.14		0.40	39.04	0.87	0.83	0.85	Hall et al. (2011)	included